LLNL-TR-416493

Equivalent Circuit Modeling of Hysteresis Motors

J. J. Nitao, E. T. Scharlemann, and B. A. Kirkendall

21 July 2009

This work performed under the auspices of the U.S. Department of Energy by Lawrence Livermore National Laboratory under Contract DE-AC52-07NA27344.

Contents

List of Figures

Summary

We performed a literature review and found that many equivalent circuit models of hysteresis motors in use today are incorrect. The model by Miyairi and Kataoka (1965) is the correct one. We extended the model by transforming it to quadrature coordinates, amenable to circuit or digital simulation.

"Hunting" is an oscillatory phenomenon often observed in hysteresis motors. While several works have attempted to model the phenomenon with some partial success, we present a new complete model that predicts hunting from first principles.

Chapter 1

Introduction to Hysteresis Motors and their Modeling

1.1 Mode of Operation

Hysteresis motors were first described by Steinmetz (1917). They are characterized by a solid rotor composed of a material having a high degree of magnetic hysteresis. The rotor shape is a cylinder or disk. Alternating current, usually polyphase, is applied to the surrounding stator coils.

All magnetic materials have some degree of hysteresis – the magnetization on a magnetic material is less when an applied external field is increasing than when it is decreasing. Consequently, the magnetization of a hysteretic material will lag behind an external oscillating field. In an hysteretic material, the magnetization will be retained after an exterrnal magnetic field is completely removed. In fact, the field has to be reversed to some extent before the magnetization returns to zero. See Fig. 1 for a plot of B vs H for a typical material.

Most ferromagnetic materials have some hysteresis, although it is often neglected for materials with a low degree of hysteresis, such as soft iron. Some materials, such as cobalt-steel alloys, have a high degree of hysteresis and are suitable for rotors of hysteresis motors.

In a hysteresis motor, the connections to the stator coil windings alternate in phase so that a rotating field is generated around the rotor, similar, in this way, to an induction motor.[1] The stator field creates poles on the rotor through magnetization. These poles follow the rotating field, and pull the rotor along. Without hysteresis (ignoring induced eddy currents for the sake of argument), the rotor would not move along with the poles – the magnetization-demagnetization cycle is a reversible process: the energy required to increase magnetization is cancelled by the energy released from demagnetization.

But, with hysteresis, the magnetized region 'wants' to remain magnetized by following the rotating stator field. The rotor material is effectively pulled along by the poles. The maximum net work available to undergo a magnetization cycle is proportional to the area inside the appropriate closed B-H hysteresis curve (Teare, 1940).[2] Figure 2 shows the counter-clockwise traversal during a single cycle. The figure also shows that a reversal in direction will result in tracing another curve.

If the load torque is sufficiently low that the required work is less than or equal to the maximum available work, then the rotor moves along with its magnetized poles. The rotor rotational speed,

[1] The synchronous mechanical angular speed of the stator field is equal to $2\omega_b/P$ where ω_b is the angular frequency (base frequency) of the polyphase input and P is the number of stator poles. This is the physical "synchronous speed" of the motor.

[2] The constant of proportionality depends purely on the number of stator coil poles and internal physical dimensions.

under steady-state conditions, is the same as the rotating field's, and the motor is said to be under *synchronous operation* with rotational mechanical speed equal to the *synchronous speed* ($= 2\omega_b/P$).

If the load torque is sufficiently high that the required work is greater than the maximum available work, then the rotor lags behind the magnetized poles and, hence, the rotor rotational speed will be less than the synchronous speed. The poles are, effectively, dragging the rotor along, but with slippage.

Although the magnetized poles on the rotor move along at the same rotational speed as the stator field, under ideal steady-state conditions, the poles lag behind the stator field by some fixed angle δ that increases with load torque. At zero load torque, the lag angle is zero. At the maximum load torque before dropping below synchronous conditions, it equals some maximum value δ_{max}. However, the actual value of the angle depends on the past history of the field due to hysteresis: the size and shape of the B-H hysteresis curve changes depending on its previous path.

The power rating of the motor is usually selected to be sufficiently high that no slip occurs under steady expected operating conditions. (Slip is defined as the difference between the rotor speed and the synchronous speed divided by the synchronous speed.) However, slip occurs during initial startup, before the synchronous speed is reached. During this period, constant torque is exerted by the motor (ignoring torque due to eddy currents).

At subsynchronous speeds, induced eddy currents in the rotor are a significant contribution to the torque in addition to that from hysteresis. At the synchronous speed under steady-state, there are no eddy currents, because there is no relative motion between the rotor and stator field. Above synchronous speeds, the eddy currents (together with the movement of the magnetized poles) cause the motor to act as an induction generator. Non-steady conditions, including oscillations about the synchronous speed will also induce eddy currents.

1.2 Hunting Phenomena

The preceding discussion mostly assumes steady-state or quasi-steady state speed conditions. As we shall see, in reality, oscillatory conditions may occur which decay very slowly to steady-state. Oscillations about the synchronous speed, in particular, are not uncommon. This phenomena is called hunting, or flutter.

The observed period of these oscillations is on the order of 1 s, with values between 1-4 s reported in the literature. The root cause of these oscillations is the oscillation of the angle δ about its equilibrium value, where δ is the angle that the magnetized poles lag behind the rotating stator field. The apparent magnetic inductances of the rotor also contribute to the oscillations.

The oscillations are system resonances that can be excited by perturbations such as changes or distortions in the electrical power supply, or sudden or cyclic changes in the mechanical load. (e.g., uneven bearing friction).

As observed in the literature, hunting oscillations in actual motors often do not decay, or decay very slowly. Although some progress has been made in understanding hunting, we believe our study is the first to give a complete model of this phenomenon.

1.3 Advantages and Disadvantages of Hysteresis Motors

Some of the advantages of hysteresis motors are:

- smooth, vibration-free operation,
- low noise,
- steady-state speed is directly controlled by the electrical input frequency,
- positive starting (non-zero torque at rest),
- no preferential orientation,
- constant torque,
- moderate current draw during startup,

- low noise.

Their disadvantages are:

- low efficiency,
- low power,
- hunting phenomenon.

1.4 Types of Hysteresis Motors

There are two main classes of hysteresis motors: cylindrical and disk.

Cylindrical hysteresis motors have a cylindrical rotor that is either wholly made of hysteretic material or can have an inner core of non-hysteretic material, e.g., part of the shaft unit (Fig. 3). The rotor is surrounded by the stator, with the rotor-stator air gap between the outer radial surface of the cylinder and inner surface of the stator.

Disk hysteresis motors have rotors shaped as an annular ring (Figs. 4 and 5). The air gap is between a flat side of the ring and the stator. The ring is often attached to a disk-shaped support centrally connected to a perpendicular shaft.

For the sake of analysis, two end classes of disk hysteresis motors have been recognized (Ishikawa and Kataoka, 1981).

A *circumferential-field* hysteresis motor has a ring support that is made of of a non-magnetic material whose magnetic permeability is assumed to be zero. The magnetic field lines in the rotor will be mostly circumferential to the ring, hence the name.

An *axial-field* hysteresis motor has ring support made of a magnetic material with an effectively infinite magnetic permeability. If the disk is thin, the field lines in the rotor will be axial to the disk (before passing through the support material), leading to the name of this motor.

1.5 Previous Work

1.5.1 Equivalent Circuits

Copeland and Slemon (1963) presented an analytical study of hysteresis motors and introduced the idea of using the fundamental harmonic response of the rotor material in reponse to the magnetizing field. They presented a conceptual equivalent circuit using a nonlinear hysteretic element.

Miyairi and T. Kataoka (1965) introduced the idea of a elliptical hysteresis curves and gave an equivalent circuit for the axial motor. Ishikawa and Kataoka (1981) extended this work to disk motors. These papers were notable in that results were derived from first principles.

Another series of papers presented or used a different set of equivalent circuits: O'Kelly (1971), Rahman (1971), Rahman and Osheiba (1990). It appears that analogies to induction or more traditional synchronous motors were presumed, and no derivation from first principles was given. We believe that the dynamic equations and equivalent circuits used in these papers are not correct. The papers of O.M.A. Badeeb (2005), Darabi et al. (2007a), and Darabi et al. (2007b) also use the same set of equations. Surprisingly, these papers refer to Miyairi and Kataoka (1965) or Ishikawa and Kataoka (1981) as their source although their equations are not the same.

Hysteresis motors are different from induction motors in that they exert a constant torque during startup (neglecting eddy effects) instead of a torque proportional to the slip. The poles on the rotor of a hysteresis motor are always moving along with rotating stator field (except for oscillations in the lag angle), whereas the poles on an induction motor are always moving at a speed different from the stator field. This means that the back-EMF characteristics of the two types of motors are not the same.

Hysteresis motors are also different from other synchronous motors in the non-linear response of the rotor field. The stator and rotor fields can-

not be treated separately and then added by linear superposition. This means that the stator and rotor inductive properties must be treated as a single unit. It follows from Miyairi and Kataoka (1965), that the effect of back-EMF from the rotor during synchronous conditions must be incorporated as part of the self-inductance of the rotor-stator system.[3] Any additional back-EMF above this baseline occurs only under slip conditions.

1.5.2 Hunting Phenomenon

Clurman (1971) investigated the phenomenon of hunting from a system viewpoint using a second order model for the oscillations. A first-principles model was not given.

Ideally, the equivalent circuit equations should be coupled to the mechanical equations of motion of the motor to predict hunting from a fundamental and mechanistic viewpoint. It was realized that hunting oscillations cannot be predicted without considering the lag angle as a dynamic degree of freedom. Ishikawa and Kataoka (1985) presented a linearized set of equations that introduced the lag angle as a time dependent variable in its own right and showed that hunting oscillations may be predicted by this method. Truong (2004) also considered the lag angle as a dynamic degree of freedom. The apparent rotor currents were considered to be constant. Darabi et al. (2007b) were the first to combine the (albeit erroneous) equivalent circuit equations with a lag angle equation of motion. However, all of these works presume that the oscillations are about a pre-computed steady state lag angle obtained from other calculations.

In this report, we propose a set of equations that automatically and continuously computes the steady state point consistent with the instantaneous current torque and load, in a natural way without substantially introducing any new equations. We believe that our work is the first to present such a method.

[3] Under synchronous conditions the magnetic field is independent of the synchronous speed since the poles are fixed on the rotor and rotate with the same speed as the stator field. Thus, a baseline self-inductance can be defined that is independent of the synchronous speed.

1.6 Contributions of this Report

The original contribution of this report are:

1. Confirm the equivalent circuit equations from Miyairi and Kataoka.
2. Derive the correct equivalent circuit equations in the stationary and rotating $dq0$ reference frames.
3. Present a model that combines the correct equivalent circuit equations with an equation for the lag angle that correctly and dynamically accounts for the steady-state due to changes in the torque output and motor load.

Chapter 2

Governing Equations and Equivalent Circuits

2.1 The Electrical Subsystem

This section describes the equivalent circuits for the stator and rotor electrical systems of a hysteresis motor based on the papers by Miyairi and Kataoka (1965, 1966), and Ishikawa and Kataoka (1981).

A balanced single-frequency, three-phase input is assumed for the motor, with voltages:[1]

$$\begin{aligned} v_a(t) &= V_o \cos(\omega_b t), \\ v_b(t) &= V_o \cos(\omega_b t - 2\pi/3), \\ v_c(t) &= V_o \cos(\omega_b t + 2\pi/3), \end{aligned} \tag{2.1}$$

and current with phase shift ψ_1:[2]

$$\begin{aligned} i_a(t) &= I_o \cos(\omega_b t + \psi_1), \\ i_b(t) &= I_o \cos(\omega_b t - 2\pi/3 + \psi_1), \\ i_c(t) &= I_o \cos(\omega_b t + 2\pi/3 + \psi_1), \end{aligned} \tag{2.2}$$

Another important assumption made in the papers is that the B-H hysteresis curve of the rotor material can be approximated by a rotated ellipse:

$$B = B_m \cos(\theta - \delta), \quad H = \frac{B_m}{\mu} \cos(\theta), \tag{2.3}$$

where θ is a parametric variable, $\mu > 0$ is an "apparent permeability", and δ is the angle by which the B-field lags the H-field, which, in this case, is rotating and is generated by the stator coils.[3]

The elliptic hysteresis curve assumption can be understood as representing the lowest angular harmonic of B within the rotor in response to the rotating sinusoidal H field. Higher order harmonics of B are neglected.

A traversal of the hysteresis curve lies on the ellipse only if the cycling is around the ellipse in the counter-clockwise motion, without any change in direction. Reversals in direction lead to movement between ellipses (see Fig. 9) and consequent changes in lag angle δ. (Despite the figure, δ always changes continuously.)

We also note that the hysteresis curve for all points on the rotor is characterized by a single value of δ. This is consistent only if one presumes the first harmonic sinusoidal assumption discussed earlier.

2.1.1 Transformation of Variables

The equivalent circuits derived in the mentioned papers are in the form of three circuits, one for each

[1] The base frequency ω_b is the actual frequency at the input bus of the motor and does not depend on the number of poles.

[2] The phase shift ψ_1 depends on the frequency as well as motor operating conditions.

[3] For a non-hysteretic, linear material, we have $B = \mu H$ where the permeability μ depends on the material. For a hysteretic material B is a nonlinear multi-valued function of H whose form depends on the material's past history.

of the three phases. They are coupled by mutual inductances between each pair of phases that arise from leakage inductances between stator coils.

Although this coupling is not a problem for a digital simulation, it complicates implementation into circuit simulation programs, such as SPICE.

The transformation to what is known as $dq0$ coordinates will be seen to decouple the mutual inductances. Another advantage is the resulting reduction of the number of solution variables from six to four.

We will use the subscript s to denote stator quantities and r to denote rotor quantities.

The 3-phase electrical inputs to the stator coils of the motor are the voltages (v_{as},v_{bs},v_{cs}) and currents (i_{as},i_{bs},i_{cs}). The $dq0$ variables are related to these variables through the linear transformation:

$$\begin{bmatrix} v_{ds} \\ v_{qs} \\ v_{0s} \end{bmatrix} = \mathbf{T}_o \begin{bmatrix} v_a \\ v_b \\ v_c \end{bmatrix}, \tag{2.4}$$

$$\begin{bmatrix} i_{ds} \\ i_{qs} \\ i_{0s} \end{bmatrix} = \mathbf{T}_o \begin{bmatrix} i_a \\ i_b \\ i_c \end{bmatrix}, \tag{2.5}$$

where the matrix $\mathbf{T}_{dq0}$ is defined as

$$\mathbf{T}_o \equiv \frac{2}{3} \begin{bmatrix} 1 & -\frac{1}{2} & -\frac{1}{2} \\ 0 & -\frac{\sqrt{3}}{2} & \frac{\sqrt{3}}{2} \\ \frac{1}{\sqrt{2}} & \frac{1}{\sqrt{2}} & \frac{1}{\sqrt{2}} \end{bmatrix}. \tag{2.6}$$

The inverse matrix is

$$\mathbf{T}_o^{-1} \equiv \begin{bmatrix} 1 & 0 & \frac{1}{\sqrt{2}} \\ -\frac{1}{2} & -\frac{\sqrt{3}}{2} & \frac{1}{\sqrt{2}} \\ -\frac{1}{2} & \frac{\sqrt{3}}{2} & \frac{1}{\sqrt{2}} \end{bmatrix}. \tag{2.7}$$

It can be shown that balanced inputs (i.e., of the form of (2.1) and (2.2)) upon transformation to $dq0$ variables, have zero voltages and currents for the 0 variables:

$$i_{0s} = v_{0s} = 0, \tag{2.8}$$

$$i_{0r} = v_{0r} = 0, \tag{2.9}$$

and, therefore, these variables can be ignored.

The above transformation is in the frame of the stator coils and is considered to be in the stationary frame. Another possibility is to use the rotating frame which moves along with the rotating stator field. The rotating frame is not convenient for implementing into circuit simulation programs because the transformation matrix depends on the angle of field rotation. However, it is convenient for digital simulation because the input currents and voltages are transformed to constants. See Sec. 4.3.1 for details.

2.1.2 Electrical Circuit Equations

As derived in Sec. 4.1, the equations for the stator-rotor electrical system in the $dq0$ stationary reference frame are

$$v_{ds} = R_s i_{ds} + \frac{d\lambda_{ds}}{dt}, \tag{2.10}$$

$$v_{qs} = R_s i_{qs} + \frac{d\lambda_{qs}}{dt}, \tag{2.11}$$

$$0 = v_{dr} = R_r i_{dr} + \frac{d\lambda_{dr}}{dt}, \tag{2.12}$$

$$0 = v_{qr} = R_r i_{qr} + \frac{d\lambda_{qr}}{dt}. \tag{2.13}$$

The "flux linkages" are given by

$$\lambda_{ds} = (L_m + L_{ls}) i_{ds} + L_m i_{dr}, \tag{2.14}$$

$$\lambda_{qs} = (L_m + L_{ls}) i_{qs} + L_m i_{qr}, \tag{2.15}$$

$$\lambda_{dr} = (L_m + L_{hr}) i_{dr} + L_m i_{ds}, \tag{2.16}$$

$$\lambda_{qr} = (L_m + L_{hr}) i_{qr} + L_m i_{qs}. \tag{2.17}$$

The quantity L_{ls} is the leakage inductance between stator coils. L_m is a form of apparent mutual inductance at the air gap between the stator and rotor, and L_{hr} is an apparent inductance due to rotor hysteresis. R_s is the stator coil resistance, and R_r is the apparent rotor resistance given by

$$\begin{aligned} R_r &\equiv \text{HarmonicAverage}\{R_h,\, R_e/s\} \\ &= \frac{1}{1/R_h + s/R_e}, \end{aligned} \tag{2.18}$$

where R_h is the contribution from hysteresis, R_e is eddy current resistance, and $s \equiv (\omega_r - \omega_b)/\omega_b$ is the motor slip. Here, ω_r is the rotor *electric* angular speed.[4]

The above equations can be rewritten in matrix notation as

$$\mathbf{V}_{dq} = \left(\mathbf{R} + \mathbf{L}_1 \frac{d}{dt}\right) \cdot \mathbf{I}_{dq}, \tag{2.19}$$

where

$$\mathbf{V}_{dq} \equiv \begin{bmatrix} v_{ds} \\ v_{qs} \\ 0 \\ 0 \end{bmatrix}, \qquad \mathbf{I}_{dq} \equiv \begin{bmatrix} i_{ds} \\ i_{qs} \\ i_{dr} \\ i_{qr} \end{bmatrix}, \tag{2.20}$$

$$\mathbf{R} \equiv \begin{bmatrix} R_s & 0 & 0 & 0 \\ 0 & R_s & 0 & 0 \\ 0 & 0 & R_r & 0 \\ 0 & 0 & 0 & R_r \end{bmatrix}, \tag{2.21}$$

$$\mathbf{L}_1 \equiv \begin{bmatrix} L_s & 0 & L_m & 0 \\ 0 & L_s & 0 & L_m \\ L_m & 0 & L_r & 0 \\ 0 & L_m & 0 & L_r \end{bmatrix}. \tag{2.22}$$

Here, we used the short-hand notation:

$$L_s \equiv L_m + L_{ls}, \qquad L_r \equiv L_m + L_{hr}. \tag{2.23}$$

2.1.3 Equivalent Circuits for the Electrical System

Fig. 6 shows the electrical circuits whose governing equations are (2.10)-(2.13). The voltages and currents are in the *dq* coordinates. The inputs in the original *abc* system are transformed using (2.6) and (2.7). Each circuit consists of LR loops connected by a common mutual inductor.

[4]Note that ω_r is not the mechanical rotor speed, which we call ω, but is related by $\omega_r = P\omega/2$, where P = no. of stator poles.

2.2 The Mechanical Motor System

2.2.1 Output Torque

The output torque of the motor is given by

$$T_e = \left(\frac{3}{2}\right)\left(\frac{P}{2}\right) L_m I_g I_r \sin\delta. \tag{2.24}$$

The magnitudes of the rotor and gap currents are defined by

$$I_r = \sqrt{i_{dr}^2 + i_{qr}^2}, \tag{2.25}$$

$$I_g = \sqrt{i_{dg}^2 + i_{qg}^2}. \tag{2.26}$$

The "air gap currents" are defined as the sum of the respective stator and rotor currents:

$$i_{dg} \equiv i_{ds} + i_{dr}, \tag{2.27}$$

$$i_{qg} \equiv i_{qs} + i_{qr}. \tag{2.28}$$

2.2.2 Equation of Mechanical Motion

The equation of motion for the rotor *electric* angular velocity ω_r is

$$J \cdot \left(\frac{2}{P}\right) \frac{d\omega_r}{dt} = T_e - T_L, \tag{2.29}$$

where J is the total moment of inertia, which includes the rotor moment of inertia. The variable ω_b is the electric angular frequency of the rotating stator field, which equals the "synchronous speed". It is equal to the angular frequency of the motor input, and is the same frequency as in (2.1)-(2.2).

The load torque T_L is some function of the true, or mechanical, angular rotor velocity ω ($=P\omega_r/2$), and includes damping terms.

The lag angle δ obeys the equation:

$$\frac{d\delta}{dt} = \left(\frac{2}{P}\right) \cdot (\omega_b - \omega_r), \tag{2.30}$$

subject to the condition:

$$|\delta| \le \delta_{max}. \tag{2.31}$$

If $|\delta| > \delta_{max}$ during solution of (2.30), then δ is reset to δ_{max} if $\delta > 0$, and $-\delta_{max}$ if $\delta < 0$.

2.2.3 Analog Circuit

Equation (2.29) for ω_r can be implemented using an LC circuit (see Fig. 7). To solve (2.29), we can use an inductor circuit with unit inductance connected to a controlled-voltage source whose output is equal to the RHS of the equation.

Another possibility for (2.29) is to use an opamp integrator whose input is a voltage source equal to the RHS and outputs δ. To avoid accumulation errors, the opamp integrator will have to be periodically restarted.

2.3 Impedance Coupling

Because the input voltages and currents to the motor must be transformed by the $dq0$ matrix transformation, appropriate buffers must be used to ensure that the input impedances of the motor stator are correct. There are two possible approaches to attain this object. The first is to use a voltage buffer with virtually-infinite input impedance, and as converter a modulated current source. Fig. 8 shows this approach. Another approach is to use a current buffer and a modulated voltage drop.

Fig. 8 also shows voltage buffers used to avoid undesired voltage drops due to their use as input to he inverse transformation circuit subsystem.

Chapter 3

Expressions for Circuit Component Parameters

3.1 Stator Coil Properties

Stator Coil Resistance

The resistance R_s is the total (DC) resistance of the stator coils for a single phase. In the laboratory, it can be easily measured directly by using an ohm-meter. An expression for R_s is given by Darabi et al. (2007a) in terms of the number of windings and wire gauge.[1] Table II in their paper has typical motor dimensions that can be substituted into their expression.

Stator Coil Leakage Inductance

Darabi et al. (2007a) give an expression for the leakage reactance X_1 of the stator coils. The desired leakage inductance L_m expressed in terms of X_1 is[2]

$$L_{ls} = \frac{X_1}{\omega_b}. \tag{3.1}$$

Again, Table II of their paper has typical motor dimensions that can be substituted into their expression.

[1] Warning: Darabi et al. use mixed units for length, leading to various powers of 10 appearing in their expressions.

[2] Note: The expression for X_1 will be seen to have a factor of ω_b, which cancels the denominator, leaving L_{ls} to be independent of ω_b.

3.2 Rotor Material Ellipse Parameters

The parameters B_m, μ, and δ_{max} define the maximal area hysteresis ellipse:

$$H = (B_m/\mu)\cos\theta, \tag{3.2}$$

$$B = B_m \cos(\theta - \delta_{max}). \tag{3.3}$$

These parameters depend on the past history, especially the largest peak value H_m ($=B_m/\mu$) of the field experienced by the rotor in the past.

Experimentally, the parameters can be estimated by applying a sinusoidally-varying field to the rotor material sample:

$$H(t) = H_m \cos\omega t, \tag{3.4}$$

where we have set $\theta = \omega t$. We then find the lowest harmonic in the measured resulting waveform for B, in the form:

$$B(t) = B_m \cos(\omega t - \delta_{max}), \tag{3.5}$$

and fit for B_m and δ_{max}. The above is done for different values of H_m. Typically, δ_{max} ranges from 30 to 50 degrees.

Darabi et al. (2007a) expands (3.3) in the form:

$$B = a_1 \cos\theta + b_1 \sin\theta, \tag{3.6}$$

where we see that

$$a_1 = B_m \cos\delta_{max}, \quad b_1 = B_m \sin\delta_{max}. \tag{3.7}$$

In Fig. 4 of their paper, Darabi et al. (2007a) have plotted a_1 versus peak H_m (= H_p in their notation) for their particular rotor material. In Fig. 3 of their paper, they plot the area E_h in the ellipse versus peak H_m. The parameter b_1 is related to E_h through

$$b_1 = \frac{E_h}{\pi H_m} \ . \tag{3.8}$$

The maximum lag angle can be found through

$$\delta_{max} = \tan^{-1}(b_1/a_1) \ , \tag{3.9}$$

and the permeability by

$$\mu = B_m/H_m \ , \tag{3.10}$$

where

$$B_m = a_1/\cos\delta_{max} \ . \tag{3.11}$$

We found that μ for their material does not vary much with H_m and has a value around 0.001.

3.3 Cylindrical Motor

The rotor core which supports the hysteretic ring is assumed to be of a non-magnetic material with zero permeability.
Rotor Gap Inductance:

$$L_m = \frac{2mK_w^2N_w^2\mu_o r_g \ell \mu}{\pi p^2 \ell_g}, \tag{3.12}$$

where

m	the number of phases,
p	the number of pole pairs (= $P/2$),
K_w	winding coefficient,
N_w	no. of stator windings per phase,
r_g	mean radius of air gap,
ℓ	axial thickness of rotor,
ℓ_g	air gap width.

Rotor Equivalent Resistance for Hysteresis:

$$R_h = \omega_b \frac{mK_w^2N_w^2V_r\mu}{\pi^2 r_r^2}\sin\delta, \tag{3.13}$$

where r_r is the mean radius of the hysteretic ring on the rotor and $V_r = 2\pi r_r t_r \ell$ is the volume of the rotor cylinder. Note that R_h is proportional to $\sin\delta$ and can be negative.
Rotor Hysteresis Inductance:

$$L_{hr} = \frac{mK_w^2N_w^2V_r\mu}{\pi^2 r_r^2}\cos\delta. \tag{3.14}$$

3.4 Axial-Field Disk Motor

Rotor Gap Inductance:

$$L_m = \frac{2mK_w^2N_w^2\mu_o r_r \ell}{\pi p^2 \ell_g}. \tag{3.15}$$

where

r_r	mean radius of rotor ring,
ℓ	$= r_o - r_i$,
r_o	outer radius of ring,
r_i	inner radius of ring.

Rotor Equivalent Resistance for Hysteresis:

$$R_h = \omega_b \frac{mK_w^2N_w^2V_r\mu}{\pi^2 p^2 t_r^2}\sin\delta. \tag{3.16}$$

Rotor Hysteresis Inductance:

$$L_{hr} = \frac{mK_w^2N_w^2V_r\mu}{\pi^2 p^2 t_r^2}\cos\delta, \tag{3.17}$$

where

V_r	volume of rotor ring (= $2\pi r_r \ell t_r$),
t_r	thickness of rotor ring.

3.5 Circumferential-Field Disk Motor

Rotor Gap Inductance:

$$L_m = \frac{2mK_w^2N_w^2\mu_o r_r \ell}{\pi p^2 \ell_g}\alpha_o, \tag{3.18}$$

where

$$\alpha_o \equiv \frac{(\beta_1^2 + 4\beta_2^2)\sin\delta}{16k_1^2k_2\beta_2}. \tag{3.19}$$

Rotor Equivalent Resistance for Hysteresis:

$$R_h = \omega_b \frac{m K_w^2 N_w^2 V_r \mu}{\pi^2 r_r^2} \alpha_r \sin\delta. \tag{3.20}$$

Rotor Hysteresis Inductance:

$$L_{hr} = \frac{m K_w^2 N_w^2 V_r \mu}{\pi^2 r_r^2} \alpha_r \cos\delta, \tag{3.21}$$

where

$$\alpha_r \equiv \frac{\beta_1^2 + 4\beta_2^2}{k_2(8\beta_1 - 16\beta_2 \cot\delta)}, \tag{3.22}$$

$$k_1 \equiv r_r/r_m, \qquad k_2 \equiv \ell/2r_r, \tag{3.23}$$

$$r_m \equiv p\sqrt{\mu \ell_g t_r/\mu_o}, \tag{3.24}$$

$$\beta_1 \equiv \ln\left\{\frac{k_1^4(1+k_2)^4 + 2k_1^2(1+k_2)^2\cos\delta + 1}{k_1^4(1-k_2)^4 + 2k_1^2(1-k_2)^2\cos\delta + 1}\right\}, \tag{3.25}$$

$$\beta_2 \equiv \tan^{-1}\left\{\frac{k_1^2(1+k_2)^2}{\sin\delta} + \cot\delta\right\} - \tan^{-1}\left\{\frac{k_1^2(1-k_2)^2}{\sin\delta} + \cot\delta\right\}. \tag{3.26}$$

To avoid division by zero in some of the above expressions when $\delta = 0$, one could use the approximation:

$$\beta_2 \approx \left[\frac{1}{k_1^2(1-k_2)^2 + \cos\delta} - \frac{1}{k_1^2(1+k_2)^2 + \cos\delta}\right]\sin\delta \tag{3.27}$$

(which holds for $\delta \approx 0$), although in numerical simulations the use of the C++/C/Fortran atan2 function in Eq. (3.26) makes this approximation unnecessary.

3.6 Effect of Eddy Currents

Rahman and Qin (1997) give the following expression for R_e for a cylindrical motor:

$$R_e = \frac{12\ell\rho}{10^4 A_h} \tag{3.28}$$

where ρ is specific resistivity and A_h is the cross-sectional area of the ring. This expression is also used by others. We have not been able to find a source for this expression.[3]

Miyairi and Kataoka (1966) derived an expression from first principles for circumferential-flux motors. The derivation is detailed in Appendix A. The expression is complex and we direct the reader to the original reference.[4]

There have been no papers published on the eddy current expression for disk motors. Since a circumferential-flux motor is similar to the circumferential-flux disk motor (Ishikawa and Kataoka 1981), the same expression for the eddy resistance can be used, with some minor modifications.

[3] Dimensionally, the expression is sound, and some form of it could be used although the numerical factors that are in the reference are puzzling. A partial explanation may be that ℓ and A_h are in mm and mm^2, respectively.

[4] The first expression for the eddy resistance in paper is for a different circuit topology than the one used in the report. The authors, then, derive the resistance for the same circuit used here.

Chapter 4

Derivation of Equations and Equivalent Circuits

4.1 Motor Electrical Circuit Equations

Under the assumption of balanced inputs, Miyairi and Kataoka (1965) have derived the governing equations for the cylindrical hysteresis motor (see Sec. A.1 of Appendix A). Ishikawa and T. Kataoka (1981) derived equations for the disk hysteresis motor. The equations have the same form for both motor types:

$$v_{as} = R_s i_{as} + \frac{d\lambda_{as}}{dt}, \tag{4.1}$$

$$v_{bs} = R_s i_{bs} + \frac{d\lambda_{bs}}{dt}, \tag{4.2}$$

$$v_{cs} = R_s i_{cs} + \frac{d\lambda_{cs}}{dt},$$

$$0 = v_{ar} = R_r i_{ar} + \frac{d\lambda_{ar}}{dt}, \tag{4.3}$$

$$0 = v_{br} = R_r i_{br} + \frac{d\lambda_{br}}{dt}, \tag{4.4}$$

$$0 = v_{cr} = R_r i_{cr} + \frac{d\lambda_{cr}}{dt}. \tag{4.5}$$

Note that there is one equation for each phase: a, b, c.

Mutual inductances between the stator coils were neglected in their papers. The flux linkages are

$$\lambda_{as} = L_{l1} i_{as} + L_m(i_{as} + i_{ar}), \tag{4.6}$$

$$\lambda_{bs} = L_{l1} i_{bs} + L_m(i_{bs} + i_{br}), \tag{4.7}$$

$$\lambda_{cs} = L_{l1} i_{cs} + L_m(i_{cs} + i_{cr}), \tag{4.8}$$

$$\lambda_{ar} = L_{hr} i_{ar} + L_m(i_{as} + i_{ar}), \tag{4.9}$$

$$\lambda_{br} = L_{hr} i_{br} + L_m(i_{bs} + i_{br}), \tag{4.10}$$

$$\lambda_{cr} = L_{hr} i_{cr} + L_m(i_{cs} + i_{cr}). \tag{4.11}$$

$$\tag{4.12}$$

Here, L_{l1} are the stator coil inductances due to leakage.

We can include mutual inductances between the stator coils by modifying the flux linkages to be:

$$\lambda_{as} = L_{l1} i_{as} + L_m(i_{as} + i_{ar}) - L_{ms}(i_{bs} + i_{cs}), \tag{4.13}$$

$$\lambda_{bs} = L_{l1} i_{bs} + L_m(i_{bs} + i_{br}) - L_{ms}(i_{as} + i_{cs}), \tag{4.14}$$

$$\lambda_{cs} = L_{l1} i_{cs} + L_m(i_{cs} + i_{cr}) - L_{ms}(i_{as} + i_{bs}), \tag{4.15}$$

where L_{ms} is the stator mutual inductance. The flux linkages for the rotor are unchanged.

In vector form, the electrical circuit equations

are

$$\boldsymbol{v}_s^{abc} = R_s \boldsymbol{i}_s^{abc} + \frac{d\boldsymbol{\lambda}_s^{abc}}{dt}, \tag{4.16}$$

$$\boldsymbol{v}_r^{abc} = R_r \boldsymbol{i}_r^{abc} + \frac{d\boldsymbol{\lambda}_r^{abc}}{dt}, \tag{4.17}$$

$$\boldsymbol{\lambda}_s^{abc} = \mathbf{L}_s^{abc} \boldsymbol{i}_s^{abc} + L_m \boldsymbol{i}_r^{abc}, \tag{4.18}$$

$$\boldsymbol{\lambda}_r^{abc} = (L_{hr} + L_m) \boldsymbol{i}_r^{abc} + L_m \boldsymbol{i}_s^{abc}, \tag{4.19}$$

$$\mathbf{L}_s^{abc} \equiv \begin{bmatrix} L_{l1}+L_m & -L_{ms} & -L_{ms} \\ -L_{ms} & L_{l1}+L_m & -L_{ms} \\ -L_{ms} & -L_{ms} & L_{l1}+L_m \end{bmatrix}, \tag{4.20}$$

$$\boldsymbol{v}_s^{abc} \equiv \begin{bmatrix} v_{as} \\ v_{bs} \\ v_{cs} \end{bmatrix}, \quad \boldsymbol{v}_r^{abc} \equiv \begin{bmatrix} v_{ar} \\ v_{br} \\ v_{cr} \end{bmatrix}, \tag{4.21}$$

$$\boldsymbol{i}_s^{abc} \equiv \begin{bmatrix} i_{as} \\ i_{bs} \\ i_{cs} \end{bmatrix}, \quad \boldsymbol{i}_r^{abc} \equiv \begin{bmatrix} i_{ar} \\ i_{br} \\ i_{cr} \end{bmatrix}. \tag{4.22}$$

4.2 Equations in the Stationary Frame

4.2.1 Transformation to dq0 Variables

The voltages and currents are transformed by the dq0 transformation:

$$\boldsymbol{v}_s^{dq0} = \mathbf{T}_o \boldsymbol{v}_s^{abc}, \quad \boldsymbol{v}_r^{dq0} = \mathbf{T}_o \boldsymbol{v}_r^{abc}, \tag{4.23}$$

$$\boldsymbol{i}_s^{dq0} = \mathbf{T}_o \boldsymbol{i}_s^{abc}, \quad \boldsymbol{i}_r^{dq0} = \mathbf{T}_o \boldsymbol{i}_r^{abc}, \tag{4.24}$$

$$\boldsymbol{v}_s^{dq0} \equiv \begin{bmatrix} v_{ds} \\ v_{qs} \\ v_{0s} \end{bmatrix}, \quad \boldsymbol{v}_r^{dq0} \equiv \begin{bmatrix} v_{dr} \\ v_{qr} \\ v_{0r} \end{bmatrix}, \tag{4.25}$$

$$\boldsymbol{i}_s^{dq0} \equiv \begin{bmatrix} i_{ds} \\ i_{qs} \\ i_{0s} \end{bmatrix}, \quad \boldsymbol{i}_r^{dq0} \equiv \begin{bmatrix} i_{dr} \\ i_{qr} \\ i_{0r} \end{bmatrix}, \tag{4.26}$$

where the matrix $\mathbf{T}_0$ is defined[1] by

$$\mathbf{T_o} \equiv \frac{2}{3} \begin{bmatrix} 1 & -\frac{1}{2} & -\frac{1}{2} \\ 0 & -\frac{\sqrt{3}}{2} & \frac{\sqrt{3}}{2} \\ \frac{1}{\sqrt{2}} & \frac{1}{\sqrt{2}} & \frac{1}{\sqrt{2}} \end{bmatrix}. \tag{4.27}$$

Its inverse is

$$\mathbf{T_o}^{-1} \equiv \begin{bmatrix} 1 & 0 & \frac{1}{\sqrt{2}} \\ -\frac{1}{2} & -\frac{\sqrt{3}}{2} & \frac{1}{\sqrt{2}} \\ -\frac{1}{2} & \frac{\sqrt{3}}{2} & \frac{1}{\sqrt{2}} \end{bmatrix}. \tag{4.28}$$

This is a particular case of a more general transformation that will be discussed later.

Writing (4.16)-(4.19) in terms of the transformed variables, we have

$$\boldsymbol{v}_s^{dq0} = R_s \boldsymbol{i}_s^{dq0} + \frac{d\boldsymbol{\lambda}_s^{dq0}}{dt}, \tag{4.29}$$

$$\boldsymbol{v}_r^{dq0} = R_r \boldsymbol{i}_r^{dq0} + \frac{d\boldsymbol{\lambda}_r^{dq0}}{dt}, \tag{4.30}$$

$$\boldsymbol{\lambda}_s^{dq0} = \mathbf{L}_s^{dq0} \boldsymbol{i}_s^{dq0} + L_m \boldsymbol{i}_r^{dq0}, \tag{4.31}$$

$$\boldsymbol{\lambda}_r^{dq0} = (L_{hr} + L_m) \boldsymbol{i}_r^{dq0} + L_m \boldsymbol{i}_s^{dq0}, \tag{4.32}$$

which is the same form, except with transformed matrix:

$$\mathbf{L}_s^{dq0} \equiv \mathbf{T}_o \mathbf{L}_s^{abc} \mathbf{T}_o^{-1} = \tag{4.33}$$

$$\begin{bmatrix} L_m+L_{l1}+L_{ms} & 0 & 0 \\ 0 & L_m+L_{l1}+L_{ms} & 0 \\ 0 & 0 & L_m+L_{l1}-2L_{ms} \end{bmatrix}. \tag{4.34}$$

[1] It is important to note that the power in terms of transformed variables is not equal to the usual sum of the voltage times current, but the expression must be multipled by a factor of 3/2. Some authors select the scale factor so that the transformation matrix is a unitary matrix (transpose = inverse) which preserves the power expression. Although we prefer this latter selection, we have stayed with the general convention.

The above follows from the identity:

$$\mathbf{T}_o \begin{bmatrix} A & -B & -B \\ -B & A & -B \\ -B & -B & A \end{bmatrix} \mathbf{T}_o^{-1} = \tag{4.35}$$

$$\begin{bmatrix} A+B & 0 & 0 \\ 0 & A+B & 0 \\ 0 & 0 & A-2B \end{bmatrix}. \tag{4.36}$$

For convenience, we define

$$L_{ls} \equiv L_{l1} + L_{ms}. \tag{4.37}$$

Note that the governing system of equations has been transformed into decoupled equations:

d-equations

$$v_{ds} = R_s i_{ds} + \frac{d\lambda_{ds}}{dt}, \tag{4.38}$$

$$0 = v_{dr} = R_r i_{dr} + \frac{d\lambda_{dr}}{dt}, \tag{4.39}$$

$$\lambda_{ds} = (L_m + L_{ls}) i_{ds} + L_m i_{dr}, \tag{4.40}$$

$$\lambda_{dr} = (L_m + L_{hr}) i_{dr} + L_m i_{ds}, \tag{4.41}$$

q-equations

$$v_{qs} = R_s i_{qs} + \frac{d\lambda_{qs}}{dt}, \tag{4.42}$$

$$0 = v_{qr} = R_r i_{qr} + \frac{d\lambda_{qr}}{dt}, \tag{4.43}$$

$$\lambda_{qs} = (L_m + L_{ls}) i_{qs} + L_m i_{qr}, \tag{4.44}$$

$$\lambda_{qr} = (L_m + L_{hr}) i_{qr} + L_m i_{qs}, \tag{4.45}$$

0-equations

$$v_{0s} = R_s i_{0s} + \frac{d\lambda_{0s}}{dt}, \tag{4.46}$$

$$0 = v_{0r} = R_r i_{0r} + \frac{d\lambda_{0r}}{dt}, \tag{4.47}$$

$$\lambda_{0s} = (L_m + L_{ls} - 3L_{ms}) i_{0s} + L_m i_{0r}, \tag{4.48}$$

$$\lambda_{0r} = (L_m + L_{hr}) i_{0r} + L_m i_{0s}. \tag{4.49}$$

If the inputs are balanced:

$$\begin{aligned} v_{as}(t) &= V_o \cos(\omega_b t), \\ v_{bs}(t) &= V_o \cos(\omega_b t - 2\pi/3), \\ v_{cs}(t) &= V_o \cos(\omega_b t + 2\pi/3), \end{aligned} \tag{4.50}$$

$$\begin{aligned} i_{as}(t) &= I_o \cos(\omega_b t + \psi_1), \\ i_{bs}(t) &= I_o \cos(\omega_b t - 2\pi/3 + \psi_1), \\ i_{cs}(t) &= I_o \cos(\omega_b t + 2\pi/3 + \psi_1), \end{aligned} \tag{4.51}$$

then, under transformation by $\mathbf{T}_o$, they become

$$\begin{aligned} v_{ds}(t) &= V_o \cos(\omega_b t), \\ v_{qs}(t) &= -V_o \sin(\omega_b t), \\ v_{0s}(t) &= 0, \end{aligned} \tag{4.52}$$

$$\begin{aligned} i_{ds}(t) &= I_o \cos(\omega_b t + \psi_1), \\ i_{qs}(t) &= -I_o \sin(\omega_b t + \psi_1), \\ i_{0s}(t) &= 0. \end{aligned} \tag{4.53}$$

From (4.46)-(4.49), we see that the rotor variables have zero values: $v_{0r} = 0$ and $i_{0r} = 0$. Therefore, under balanced inputs, we may ignore these variables and their corresponding equations.

Summarizing the advantages of the dq0 transformation:

- The dq0 transformation diagonalizes the matrix of mutual inductances between that stator coils.
- The equations are decoupled into three independent subsystems. Each subsystem corresponds to a separate circuit. This simplifies their implementation into a circuit simulation program.
- Balanced 3-phase inputs are transformed to 2-phase inputs.
- For balanced inputs, the number of state variables (and equations) are reduced from six to four.

4.2.2 Equivalent Circuit for the Electrical Motor System

The equations for the ds variables is

$$\begin{aligned} v_{ds} &= R_s i_{ds} + \frac{d\lambda_{ds}}{dt}, \\ &= R_s i_{ds} + L_{ls} \frac{di_{ds}}{dt} + L_m \frac{d(i_{ds} + i_{dr})}{dt}. \end{aligned} \tag{4.54}$$

Each term in the RHS of this equation corresponds to the voltage drop of the following components connected in series: resistor R_s, inductor L_{ls}, and a mutual inductor L_m with total current $i_{ds} + i_{dr}$ corresponding to connection with the subcircuit for the dr variables with current i_{dr}.

A similar observation holds for the qs equation.

The equation for the dr variables is

$$\begin{aligned} 0 &= R_r i_{dr} + \frac{d\lambda_{dr}}{dt}, \\ &= R_r i_{dr} + L_{lh}\frac{di_{dr}}{dt} + L_m\frac{d(i_{ds}+i_{dr})}{dt}. \end{aligned} \tag{4.55}$$

Similar to the ds equation, this equation describes an electrical subcircuit with the following components connected in series: resistor R_r, inductor L_{lh}, a mutual inductor L_m interacting with the subcircuit for the ds variables. The same type of circuit also applies to the qr equation.

Fig. 6 shows diagrams of the resulting equivalent circuits.

4.2.3 Motor Torque Expression

In Appendix B, we derive the following expression for the torque output:

$$T_e = \left(\frac{m}{2}\right)\left(\frac{P}{2}\right) L_m I_g I_r \sin\delta. \tag{4.56}$$

The magnitude of the rotor and gap currents are defined as

$$I_r = \sqrt{i_{dr}^2 + i_{qr}^2}, \tag{4.57}$$

$$I_g = \sqrt{i_{dg}^2 + i_{qg}^2}. \tag{4.58}$$

The "gap currents", which pass through the inductor L_m, are defined by[2]

$$i_{dg} \equiv i_{ds} + i_{dr}, \tag{4.59}$$

$$i_{qg} \equiv i_{qs} + i_{qr}. \tag{4.60}$$

[2]Note that our rotor currents i_{dr}, i_{qr} have an opposite sign to Miyairi and Kataoka's definition. In their notation the gap currents are differences between the stator and rotor currents instead of our sums.

Also in the Appendix, we show that an equivalent expression (when $m = 3$) for the torque output, in terms of the flux linkages and currents, is

$$T_e = \left(\frac{3}{2}\right)\left(\frac{P}{2}\right)(\lambda_{qr} i_{dr} - \lambda_{dr} i_{qr}). \tag{4.61}$$

This expression is not as well-behaved numerically because it relies on the cancellation of the phases of two cross-correlations, which may, in some cases, be large, but their difference may be small.

4.2.4 Equation for the Rotor Speed

The equation of motion of the motor is found using the well-known formula for the conservation of angular momentum:

$$J\frac{d\omega}{dt} = (T_e - T_L), \tag{4.62}$$

where ω is the mechanical angular velocity of the rotor. The moment of inertia J is the sum of the moments of inertia of the external load and the rotor. The external load torque T_L is a function of the angular velocity ω and includes any damping terms, such as that due to bearing friction.

The electric angular velocity ω_r is related to the mechanical angular velocity through

$$\omega_r = \left(\frac{P}{2}\right)\cdot\omega. \tag{4.63}$$

In terms of the electric angular velocity, the equation of motion becomes:

$$J\cdot\left(\frac{2}{P}\right)\frac{d\omega_r}{dt} = (T_e - T_L). \tag{4.64}$$

4.2.5 Equation for the Lag Angle

Recall that the lag angle is the angular difference between the magnetic rotating field and the magnetized poles. When the magnitude of the lag angle δ is within the range:

$$|\delta| \le \delta_{max}, \tag{4.65}$$

its time derivative is given by

$$\frac{d\delta}{dt} = \left(\frac{2}{P}\right)(\omega_b - \omega_r). \tag{4.66}$$

When the lag angle δ determined by Eq. (4.66) is outside its range, it must be reset to either δ_{max} or $-\delta_{max}$, depending on the sign of δ.

The hysteresis resistance R_{hr} was seen to be proportional to $\sin\delta$. With sufficient damping, the equation of motion will automatically adjust δ to an equilibrium point so that the resulting resistance R_h gives the rotor currents such that the output torque T_e (which depends on R_h and, hence, on δ) equals the load torque T_L.

It can be shown that under steady conditions the output torque is proportional to R_h. Increasing δ will lead to higher torque until the maximum torque is reached at δ_{max}. There will be a δ such that the exerted torque equals the load as long as the load does not exceed the maximum exerted torque.

If rotor damping is insufficient, the lag angle δ will oscillate about the equilibrium point, giving rise to the hunting phenomenon.

Note that R_h will become negative for negative δ and, therefore, behaves as a voltage source, which corresponds to the hysteresis motor acting as a generator. The negative torque generated acts to restore the lag angle to a non-negative value. In some cases, the angle may oscillate back and forth between negative and positive values.

4.2.6 Analog Circuit for Equations of Motion

Equation (4.63) for ω_r can be implemented using and LC circuit (see Fig. 7). To solve (4.66), we can use an inductor circuit with unit inductance connected to a controlled-voltage source whose output is equal to the RHS of the equation.

Another possibility for solving (4.66) is to use an opamp integrator whose input is a voltage source equal to the RHS of (4.66) and whose output is δ. To avoid accumulation errors, the opamp integrator will have to be periodically restarted.

4.3 Equations in the Rotating Frame

We now show how to transform the electrical system equations to the frame of the stator field which is rotating with electric angular speed ω_b, equal to the angular frequency of the motor input.

4.3.1 Transformation to the Rotating Frame

The general dq0 transformation to a frame rotating with angle $\theta = \theta(t)$ is given by[3]

$$\mathbf{T}_\theta \equiv \frac{2}{3}\begin{bmatrix} \cos\theta & \cos(\theta - \frac{2\pi}{3}) & \cos(\theta + \frac{2\pi}{3}) \\ \sin\theta & \sin(\theta - \frac{2\pi}{3}) & \sin(\theta + \frac{2\pi}{3}) \\ \frac{1}{\sqrt{2}} & \frac{1}{\sqrt{2}} & \frac{1}{\sqrt{2}} \end{bmatrix}, \tag{4.67}$$

The matrix $\mathbf{T}_o$ for the stationary frame is a special case with $\theta = 0$.

The inverse matrix is

$$\mathbf{T}_\theta{}^{-1} \equiv \begin{bmatrix} \cos\theta & \sin\theta & \frac{1}{\sqrt{2}} \\ \cos(\theta - \frac{2\pi}{3}) & \sin(\theta - \frac{2\pi}{3}) & \frac{1}{\sqrt{2}} \\ \cos(\theta + \frac{2\pi}{3}) & \sin(\theta + \frac{2\pi}{3}) & \frac{1}{\sqrt{2}} \end{bmatrix}. \tag{4.68}$$

Interestingly, Eq. (4.36) still holds. That is,

$$\mathbf{T}_\theta \begin{bmatrix} A & -B & -B \\ -B & A & -B \\ -B & -B & A \end{bmatrix} \mathbf{T}_\theta^{-1} = \tag{4.69}$$

$$\begin{bmatrix} A+B & 0 & 0 \\ 0 & A+B & 0 \\ 0 & 0 & A-2B \end{bmatrix}. \tag{4.70}$$

We now transform the abc variables to the rotating $dq0$ frame by

$$\boldsymbol{v}_s^{dq0} = \mathbf{T}_\theta \boldsymbol{v}_s^{abc}, \quad \boldsymbol{v}_r^{dq0} = \mathbf{T}_\theta \boldsymbol{v}_r^{abc}, \tag{4.71}$$

$$\boldsymbol{i}_s^{dq0} = \mathbf{T}_\theta \boldsymbol{i}_s^{abc}, \quad \boldsymbol{i}_r^{dq0} = \mathbf{T}_\theta \boldsymbol{i}_r^{abc}. \tag{4.72}$$

[3]The angle θ is an electric angle, not physical angle.

Written with these variables, Eqs. (4.16)-(4.19) become

$$\boldsymbol{v}_s^{dq0} = R_s \boldsymbol{i}_s^{dq0} + \mathbf{T}_\theta \frac{d}{dt} \mathbf{T}_\theta^{-1} \boldsymbol{\lambda}_s^{dq0}, \tag{4.73}$$

$$\boldsymbol{v}_r^{dq0} = R_r \boldsymbol{i}_r^{dq0} + \mathbf{T}_\theta \frac{d}{dt} \mathbf{T}_\theta^{-1} \boldsymbol{\lambda}_r^{dq0}, \tag{4.74}$$

$$\boldsymbol{\lambda}_s^{dq0} = \mathbf{L}_s^{dq0} \boldsymbol{i}_s^{dq0} + L_m \boldsymbol{i}_r^{dq0}, \tag{4.75}$$

$$\boldsymbol{\lambda}_r^{dq0} = (L_{hr} + L_m) \boldsymbol{i}_r^{dq0} + L_m \boldsymbol{i}_s^{dq0}, \tag{4.76}$$

where $\mathbf{L}_s^{dq0}$ is still given by (4.34).

It can be shown that[4]

$$\mathbf{T}_\theta \frac{d}{dt} \mathbf{T}_\theta^{-1} = \begin{bmatrix} 0 & -d\theta/dt & 0 \\ d\theta/dt & 0 & 0 \\ 0 & 0 & 0 \end{bmatrix}. \tag{4.77}$$

Since the frame is rotating with the stator field, we have that

$$\theta = \omega_b t. \tag{4.78}$$

Thus,

$$\mathbf{T}_\theta \frac{d}{dt} \mathbf{T}_\theta^{-1} = \begin{bmatrix} 0 & -\omega_b & 0 \\ \omega_b & 0 & 0 \\ 0 & 0 & 0 \end{bmatrix}. \tag{4.79}$$

Consequently, the equations may be written as

d-equations

$$v_{ds} = R_s i_{ds} + \frac{d\lambda_{ds}}{dt} - \omega_b \lambda_{qs}, \tag{4.80}$$

$$0 = v_{dr} = R_r i_{dr} + \frac{d\lambda_{dr}}{dt} - \omega_b \lambda_{qr}, \tag{4.81}$$

$$\lambda_{ds} = (L_m + L_{ls}) i_{ds} + L_m i_{dr}, \tag{4.82}$$

$$\lambda_{dr} = (L_m + L_{hr}) i_{dr} + L_m i_{ds}, \tag{4.83}$$

q-equations

$$v_{qs} = R_s i_{qs} + \frac{d\lambda_{qs}}{dt} + \omega_b \lambda_{ds}, \tag{4.84}$$

$$0 = v_{qr} = R_r i_{qr} + \frac{d\lambda_{qr}}{dt} + \omega_b \lambda_{dr}, \tag{4.85}$$

$$\lambda_{qs} = (L_m + L_{ls}) i_{qs} + L_m i_{qr}, \tag{4.86}$$

$$\lambda_{qr} = (L_m + L_{hr}) i_{qr} + L_m i_{qs}, \tag{4.87}$$

0-equations

$$v_{0s} = R_s i_{0s} + \frac{d\lambda_{0s}}{dt}, \tag{4.88}$$

$$0 = v_{0r} = R_r i_{0r} + \frac{d\lambda_{0r}}{dt}, \tag{4.89}$$

$$\lambda_{0s} = (L_m + L_{ls} - 3L_{ms}) i_{0s} + L_m i_{0r}, \tag{4.90}$$

$$\lambda_{0r} = (L_m + L_{hr}) i_{0r} + L_m i_{0s}. \tag{4.91}$$

If the inputs are balanced, then the stator inputs given by (4.50) and (4.51) become

$$v_{ds} = V_o \cos\psi_1, \quad v_{qs} = 0, \quad v_{0s} = 0, \tag{4.92}$$

$$i_{ds} = I_o \cos\psi_2, \quad i_{qs} = 0, \quad i_{0s} = 0. \tag{4.93}$$

To summarize, upon transforming to a frame rotating with the stator field, we have that

- The mutual inductance matrix is diagonalized as before.
- But, there are intercoupling terms between the d and q equations: $-\omega_b \lambda_{qs}$ and $\omega_b \lambda_{ds}$ in the stator equations and $-\omega_b \lambda_{qr}$ and $\omega_b \lambda_{dr}$ in the rotor equations.
- Balanced inputs are transformed to D.C. voltages and currents, making analysis and digital simulation easier.
- Under balanced inputs, the number of state variables is, again, reduced from six to four.
- Implementation into a circuit simulation program is cumbersome because the entries in the transformation matrix T_θ, which are needed to transform variables back and forth, are sinusoidal functions of time.

4.3.2 Equivalent Circuits for the Rotating Frame

By examining the equations, we find that the equivalent circuits are the same as that for the stationary frame, except with the addition of voltage sources $-\omega_b \lambda_{qs}$ and $-\omega_b \lambda_{qr}$ to the s and r loops, respectively, in the d circuit, and the addition of voltage sources $\omega_b \lambda_{ds}$ and $\omega_b \lambda_{dr}$ to the s and r loops, respectively, in the q circuit.

[4] This and other complicated matrix identities in this report were checked using the symbolic mathematics computer program called Maxima, which is an open source descendant of the well-established DOE Macsyma program.

4.3.3 Output Torque for the Rotating Frame

In Appendix B, we show that the output torque is given by

$$T_e = \left(\frac{m}{2}\right)\left(\frac{P}{2}\right) L_m I_g I_r \sin\delta, \tag{4.94}$$

which is the same form as for the stationary frame. The rotor and gap currents (in the rotating frame) are defined as

$$I_r = \sqrt{i_{dr}^2 + i_{qr}^2}, \tag{4.95}$$

$$I_g = \sqrt{i_{dg}^2 + i_{qg}^2}, \tag{4.96}$$

$$i_{dg} \equiv i_{ds} + i_{dr}, \tag{4.97}$$

$$i_{qg} \equiv i_{qs} + i_{qr}. \tag{4.98}$$

In the Appendix we also show that the torque output for three phase input is also given by

$$T_e = \left(\frac{3}{2}\right)\left(\frac{P}{2}\right)(\lambda_{qr} i_{dr} - \lambda_{dr} i_{qr}). \tag{4.99}$$

As mentioned before, this expression is not well-behaved numerically because it relies on the cancellation between two cross-correlations as the other formula does not.

4.3.4 Equations of Mechanical Motion

The equations of mechanical motion for ω_r and δ are the same as for the stationary frame.

Chapter 5

Preliminary Simulations

We perfomed digital simulations, solving the equations (4.80) - (4.87) in the rotating frame with the balanced voltage input in the form of (4.92). An ordinary differential equation solver RK45 written by H. A. Watt and L. F. Shampine was used for the solution. It implements the Fehlberg-Runge-Kutta method, which has automatic time stepping.

The motor parameters used in the simulations are given in Table 5.1. The load torque used is

$$T_L = A + B\omega|\omega|, \tag{5.1}$$

where

$$A = 5.66 \times 10^{-4}\text{N-m}, \tag{5.2}$$

$$B = 9.45 \times 10^{-7}\text{N-m-s}^2. \tag{5.3}$$

Fig. 10 shows the simulation neglecting the effect of eddy currents ($R_e = \infty$) when the motor starts from zero velocity. Note the constant output torque T_e until synchronous speed is reached. The lag angle δ maintains its maximum value δ_{max} during the startup period. The stator input current I_s, as well as the apparent rotor current I_r is also constant during this time period.

After the motor reaches synchronous speed, oscillations are seen to occur in the torque, lag angle, and current. There are also oscillations in the motor speed ω about the synchronous speed, although it is only barely visible due to the vertical scale of the graph.

Fig. 11 shows the simulation with eddy currents, where we have set $R_e = 1\ \Omega$. The torque during startup is about 25% higher due to the motor acting partly as an induction motor. The stator and rotor currents are also higher by that amount. Synchronous speed is reached about 50 s faster than in the no-eddy current case. As the synchronous speed is reached, eddy currents become less of a factor. The inclusion of eddy currents appears to increase damping. The actual magnitude of the eddy currents depends on R_e, which we have chosen arbitrarily.

Table 5.1: Disk Motor Parameters

P	2
m	3
ω_b	$60\times2\pi$ (rad/s)
δ_{max}	40°
t_r	0.003 m
r_o	0.15 m
r_i	0.07 m
ℓ	0.08 m
ℓ_g	0.001 m
K_w	0.8
N_w	200
J	0.10 (kg-m^2)
R_e	1.0 Ω
R_s	2.0 Ω
L_{ls}	0.01 H
V_o	70 V
μ	0.001 N/A^2

Chapter 6

Dynamic Equations Directly from the Equivalent Circuit

The dynamic hysteresis motor equations (2.10) through (2.30) provide a connection with previous discussions of hysteresis motors (Rahman (1971), Badeeb (2005), and Darabi, et al. (2008)). The equations illustrate the importance of including a dynamical equation for lag angle δ and of including the variation of R_r and L_{hr} with δ, effects that appear not to be included in the references but which are essential to (among other things) maintaining non-zero torque at synchronism.

An alternative and much simpler set of equations comes from the equivalent circuit of Fig. 6, using the complex impedances

$$\mathbf{Z}_g = j\omega_b L_m \ , \tag{6.1}$$

$$\mathbf{Z}_r = R_r + j\omega_b L_{hr} \ , \tag{6.2}$$

$$\mathbf{Z}_s = R_s + j\omega_b L_{ls} \ , \tag{6.3}$$

and total circuit impedance

$$\mathbf{Z} = \mathbf{Z}_s + \frac{1}{1/\mathbf{Z}_g + 1/\mathbf{Z}_r} \ . \tag{6.4}$$

The complex input voltage $\mathbf{V} = v_{ds} + jv_{qs} = |\mathbf{V}|e^{j\omega_b t}$ produces the current

$$\mathbf{I}_s = \mathbf{V}/\mathbf{Z} \tag{6.5}$$

with components through the two parallel branches of

$$\mathbf{I}_g = (\mathbf{V} - \mathbf{Z}_s\mathbf{I}_s)/\mathbf{Z}_g \quad \text{through } L_m \tag{6.6}$$

and

$$\mathbf{I}_r = (\mathbf{V} - \mathbf{Z}_s\mathbf{I}_s)/\mathbf{Z}_r \quad \text{through } R_r \text{ and } L_{hr} \ ; \tag{6.7}$$

this $\mathbf{I}_r$ flows in the direction opposite to the i_{dr} and i_{qr} shown in Fig. 6.

The torque is the same as previously, using the magnitudes $|\mathbf{I}_r|$ and $|\mathbf{I}_g|$:

$$T_e = \left(\frac{3}{2}\right)\left(\frac{P}{2}\right) L_m |\mathbf{I}_r||\mathbf{I}_g| \sin\delta \ . \tag{6.8}$$

The only differential equations then to solve are (2.29) for ω_r and (2.30) for δ; δ determines R_r and L_{hr} above.

Numerical simulation of these equations gives the same results as the more complicated set previously developed (Fig. 12), but with better stability properties for zero load torque after synchronism (specifically, for $R_r < 0$, which occurs when $\sin\delta < 0$), as shown in Fig. 13.

The equations above explicitly enforce the phase and amplitude relations between $\mathbf{I}_g$ and $\mathbf{I}_r$ implied by the circuit of Fig. 6, whereas Eqs. (2.10) through (2.30) do not.

Chapter 7

Hysteresis Loops and δ

Eq. (2.30) for δ implicitly assumes that when $-\delta_{max} < \delta < \delta_{max}$, the lag angle ($\delta$) behaves as a fixed point on the rotor and moves with the rotor. In reality, δ is determined by the behavior of the rotor material hysteresis loop when the dH/dt in the material changes sign while $|H| < |H_{max}|$, as happens at point 1 in Fig. 2.

We use the hysteresis model of Potter and Schmulian (1971), for which the magnetization M as a function of H is parameterized by α, with

$$M(H;\alpha) = M_s \left\{ \operatorname{sgn}\alpha - \alpha \left[1 + \tanh\left(\frac{H_c - H\operatorname{sgn}\alpha}{H_c} \tanh^{-1} S \right) \right] \right\} \tag{7.1}$$

where $\operatorname{sgn}\alpha = 1$ if $\alpha > 0$ and -1 if $\alpha < 0$, H_c is the coercivity, M_s is the saturation magnetization, $S = M_r/M_s$ is the "squareness parameter", and M_r is the remanent magnetization. The parameter α can take on values between -1 and 1, and sets the size of the hysteresis loop.

If, at a value H_m, H reverses its direction of change before the extrema of the hysteresis loop (remagnetization), the material appears on a new magnetization curve $M(H;\alpha')$, with

$$\alpha' = -\frac{2\operatorname{sgn}\alpha - \alpha\{1 + \tanh[(1 - H_m \operatorname{sgn}\alpha/H_c)\tanh^{-1} S]\}}{1 + \tanh[(1 + H_m \operatorname{sgn}\alpha/H_c)\tanh^{-1} S]} \tag{7.2}$$

For 36% cobalt steel, $M_s = 1.63$ T, $B_r = 0.975$ T, and $H_c = 1.909 \times 10^4$ A/m. For a peak H of 5×10^4 A/m, the hysteresis curve looks as shown in Fig. 14, and the behavior of δ as the rotor passes through synchronism is shown in Fig. 15. The hysteresis loops at intermediate values of δ are shown in Fig. 16. The difference between the two outer loops ($delta = \pm 0.32$) in the figure is the direction of hysteresis loop traversal. We note that a simple straight-line approximation for δ in Fig. 15 would put a factor of 0.2 in front of the r.h.s. of (2.30). The only significant effect of that factor on the previous simulations is to lengthen the period of "hunting" that appears after synchronism.

List of Important Symbols (in SI Units)

i	current (A)
j	$\sqrt{-1}$
ℓ	axial length or thickness of rotor (m)
ℓ_g	air gap thickness (m)
m	no. of electrical phases in the input
p	no. of pole pairs ($= P/2$)
r_g	mean radius of air gap region for cylindrical motors (m)
r_i	inner rotor ring radius (m)
r_o	outer rotor ring radius (m)
t	time (s)
t_r	disk thickness (m)
v	voltage (V)
B	magnetic field (T=V-s/m^2)
H	magnetizing field (A/m)
I	current magnitude (A)
J	moment of inertia of rotor plus load (kg-m^2)
K_w	winding coefficient
L_{hr}	apparent hysteresis inductance (H)
L_{ls}	stator leakage inductance (H)
L_m	apparent air gap inductance (H)
N_w	winding number
P	no. of poles
R_e	apparent eddy resistance (Ω)
R_r	apparent rotor resistance (Ω)
R_s	stator resistance (Ω)
T_e	motor torque output (N-m)
T_L	load torque (N-m)
V	voltage magnitude (V)
V_r	volume of rotor (m^3)
δ	lag angle between poles and rotating field (rad)
λ	flux linkage (V-s)
μ	permeability (H/m=N/A^2)
μ_o	permeability of free space, $4\pi \times 10^{-7}$ (H/m)
ω	actual rotor (mechanical) angular speed (rad/s)
ω_b	base angular frequency of electrical input (rad/s)
ω_r	rotor electrical angular speed, $= (P/2)\omega$ (rad/s)

References

O. M. A. Badeeb (2005), Investigation of the dynamic performance of hysteresis motors using Matlab/SIMULINK, *J. Elec. Eng., 56,* 106-109.

S. Clurman (1971), On hunting in hysteresis motors and new damping techniques, *IEEE Trans. Magnetics, 7*, no. 3, 512-517.

M. A. Copeland, G. R. Slemon (1963), An analysis of the hysteresis motor I – analysis of the idealized machine, *IEEE Trans. Power App. Sys., 82,* no. 65, 34-42.

M. A. Copeland, G. R. Slemon (1964), An analysis of the hysteresis motor II – the circumferential-flux machine, *IEEE Trans. Power App. Sys., 83,* no. 6, 619-625.

A. Darabi, T. Ghanbari, M. Rafiei, H. Lesani (2008), M. Sanati-Moghadam, Dynamic performance analysis of hysteresis motors by a linear time-varying model, *Iranian Journal of Electrical and Electronic Engineering, 4,* no. 4, 202-215.

A. Darabi, H. Lesani, T. Ghanbari, A. Akhavanhejazi (2007a), Modeling and optimum design of disk-type hysteresis motors, Proc. Inter. Conf. Elect. Mach. and Sys., Oct. 8-11, 2007, Seoul, Korea, 998-1002.

A. Darabi, M. Rafiei, T. Ghanbari (2007b), Hunting in Hysteresis Motors, Impact of Supply, Proc. Inter. Conf. Elect. Mach. and Sys., Oct. 8-11, 2007, Seoul, Korea, 1715-1718.

T. Ishikawa and T. Kataoka (1981), Basic analysis of disc-type hysteresis motors, *Elec. Engng. Japan, 101,* no. 6, 659-666.

T. Ishikawa and T. Kataoka (1985), Stability analysis of voltage source inverter-fed hysteresis motor, *Elec. Engng. Japan, 105,* no. 1, 417-424.

S. Miyairi, T. Kataoka (1965), A basic equivalent circuit of the hysteresis motor , *Elect. Engng. Japan (USA), 85*, 41-50.

S. Miyairi, T. Kataoka (1966), Analysis of hysteresis motors considering eddy current effects, *Elect. Engng. Japan (USA), 86*, no. 6, 67-77.

D. O'Kelly (1969), Eddy-current and hysteresis effects in rotating machines, *Proc. Inst. Elec. Eng., 116,* no. 3, London, 391-395.

D. O'Kelly (1971), Equivalent circuits and single-phase induction and hysteresis motors, *IEEE Trans. Power App. and Sys., PAS-90,* no. 1, 279-288.

R. I. Potter, R. J. Schmulian (1971), Self-Consistently Computed Magnetization Patterns in Thin Magnetic Recording Media, *IEEE Trans. Magnetics, MAG-7*, no. 4, 873-880.

M. A. Rahman (1971), Analytical models of polyphase hysteresis motors, *IEEE Trans. Power Apparatus and Systems, PAS-92,* no. 1, 237-242.

M. A. Rahman, A. M. Osheiba (1990), Dynamic performance prediction of polyphase hysteresis motors, *IEEE Trans. Industry Appl., 26,* 1026-1033.

M. A. Rahman, R. Qin (1997), A permanent magnet hysteresis hybrid synchronous motor for electrical vehicles, *IEEE Trans. Indust. Elec., 44,* 46-53.

S. D. T. Robertson, S. Z. G. Zaky (1969), Analysis of the hysteresis machine - Part I, *IEEE Trans. Power App. Sys., PAS-88,* no. 4, 474-484.

C. P. Steinmetz (1917), *Theory and Calculations of Electrical Apparatus,* McGraw-Hill, N. Y. (contents on Google books)

S. Tadakuma, S. Tanaka, J. Inagaki (1972), Hysteresis motors controlled by inverters, *Elect. Engng. Japan, 92,* 619-626.

B. R. Teare (1940), Theory of hysteresis-motor torque, *AIEE Trans., 59,* 907-912.

C. K. Truong (2004), *Analysis of Hunting in Synchronous Hysteresis Motor,* Master's Thesis, MIT Dept. of EECS. (http://web.mit.edu/cktruong/www/Thesis%201-23-04.pdf)

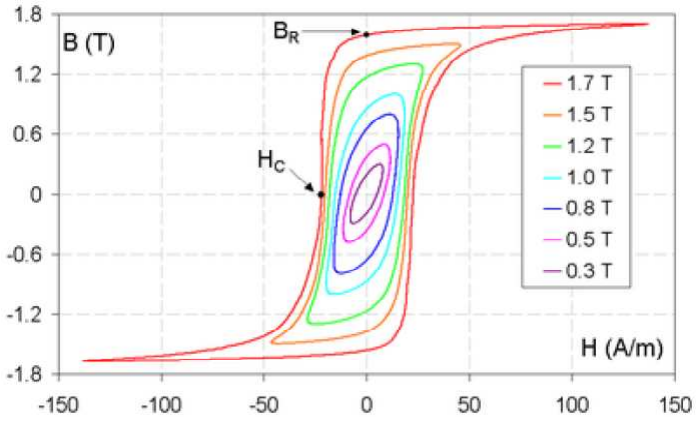

Figure 1: A family of B-H hysteresis loops for grain-oriented electrical steel. B_R is called the remanance and H_C is the coercivity. Traversal direction during a complete cycle is counterclockwise (from Wikipedia).

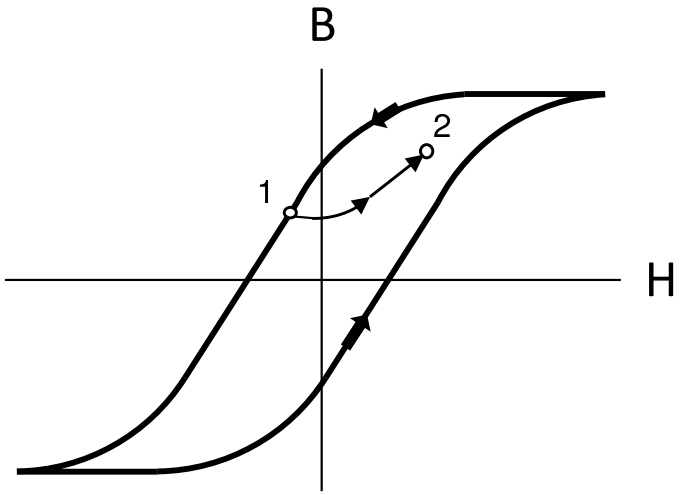

Figure 2: Traversal on the magnetic hysteresis curve.

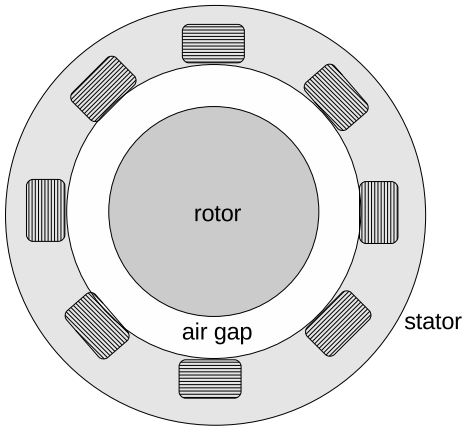

Figure 3: Cross-sectional view of a cylindrical hysteresis motor.

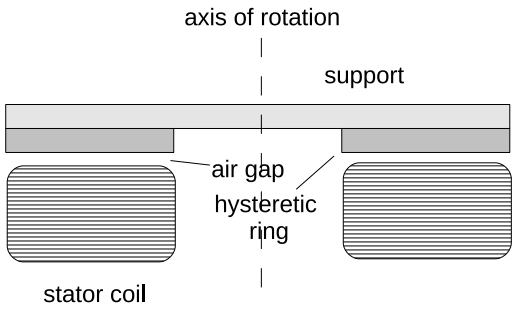

Figure 4: Cross-sectional view of disk hysteresis motor.

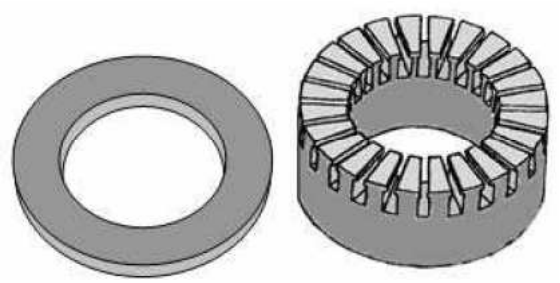

Figure 5: Rotor and stator core assembly for a disk hysteresis motor (from Darabi et al., 2007a).

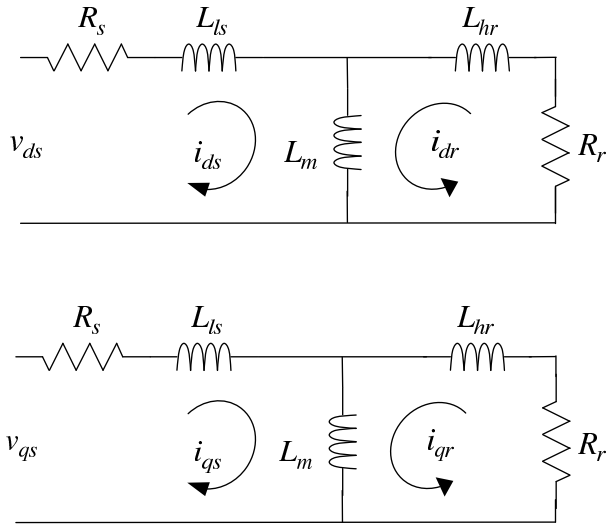

Figure 6: Equivalent circuits for the electrical system of a hysteresis motor in dq0 coordinates for the stationary frame

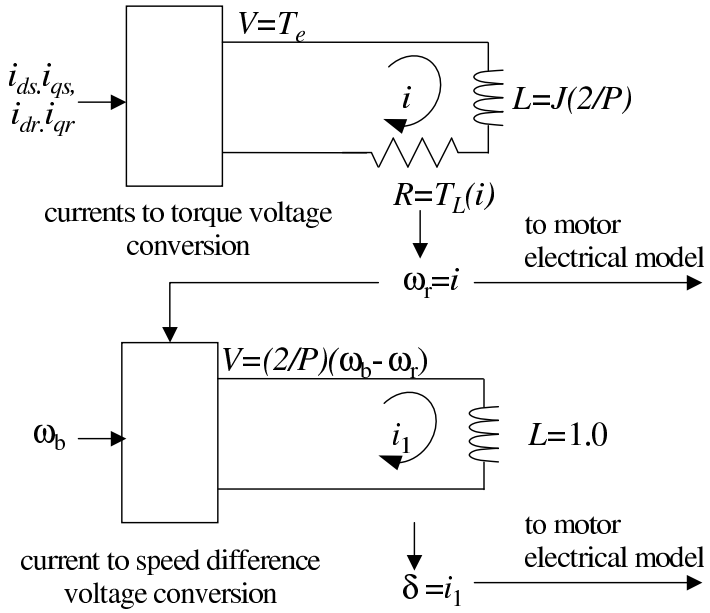

Figure 7: Analog circuit representing the mechanical motor in purely nominally synchronous mode

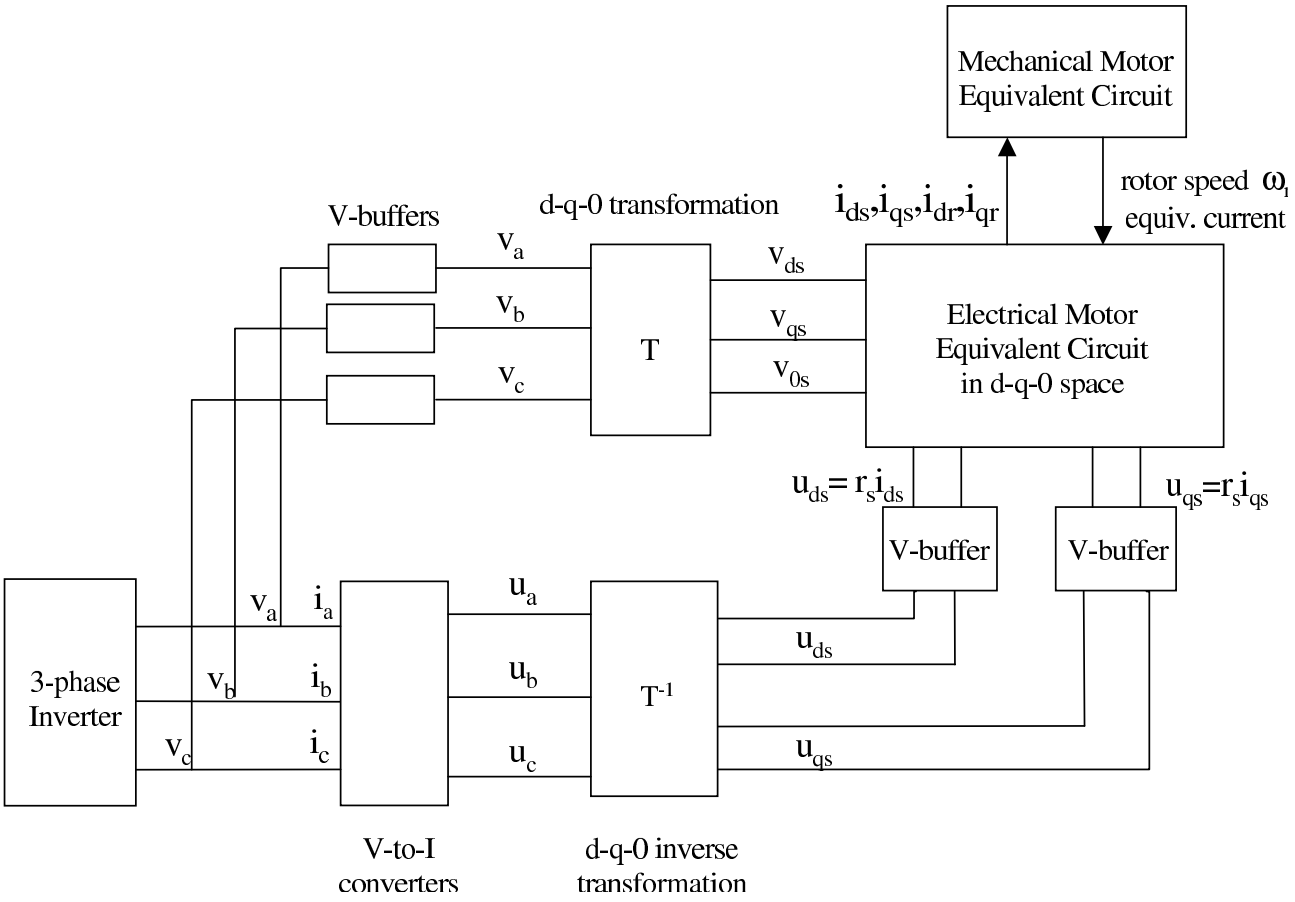

Figure 8: Diagram of the system model components

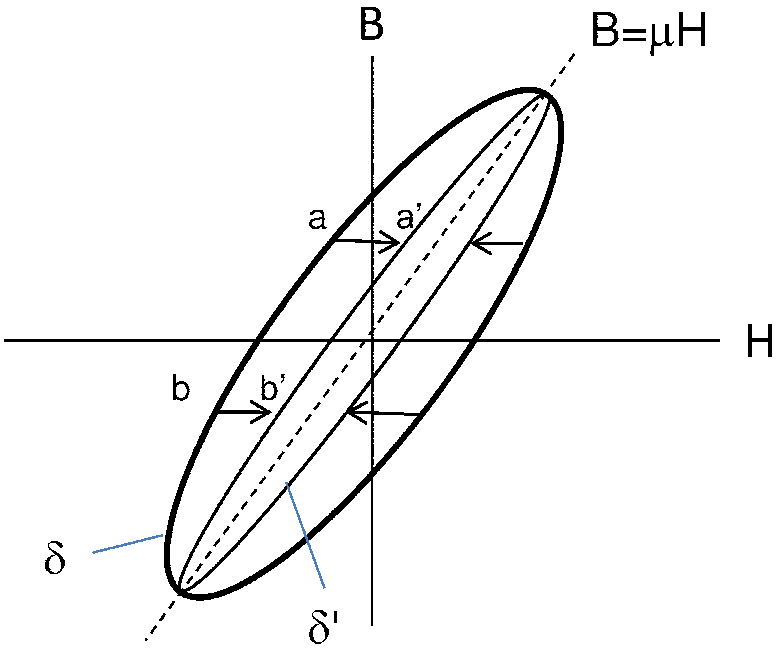

Figure 9: Moving between elliptical curves, $\delta' < \delta$.

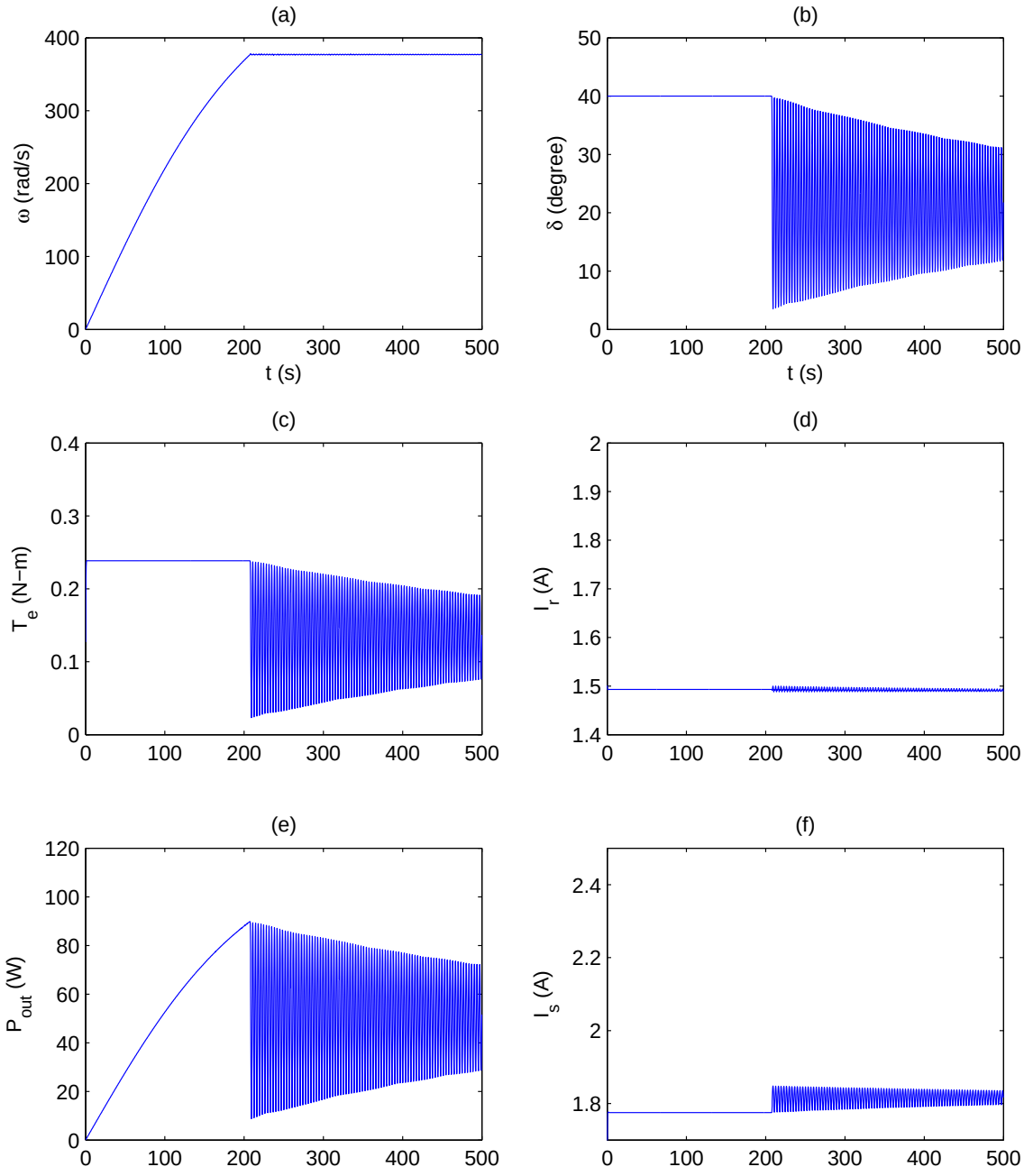

Figure 10: Simulation neglecting eddy currents: (a) mechanical angular speed, (b) lag angle, (c) output torque, (d) rotor current magnitude, (e) mechanical output power, (f) stator current magnitude.

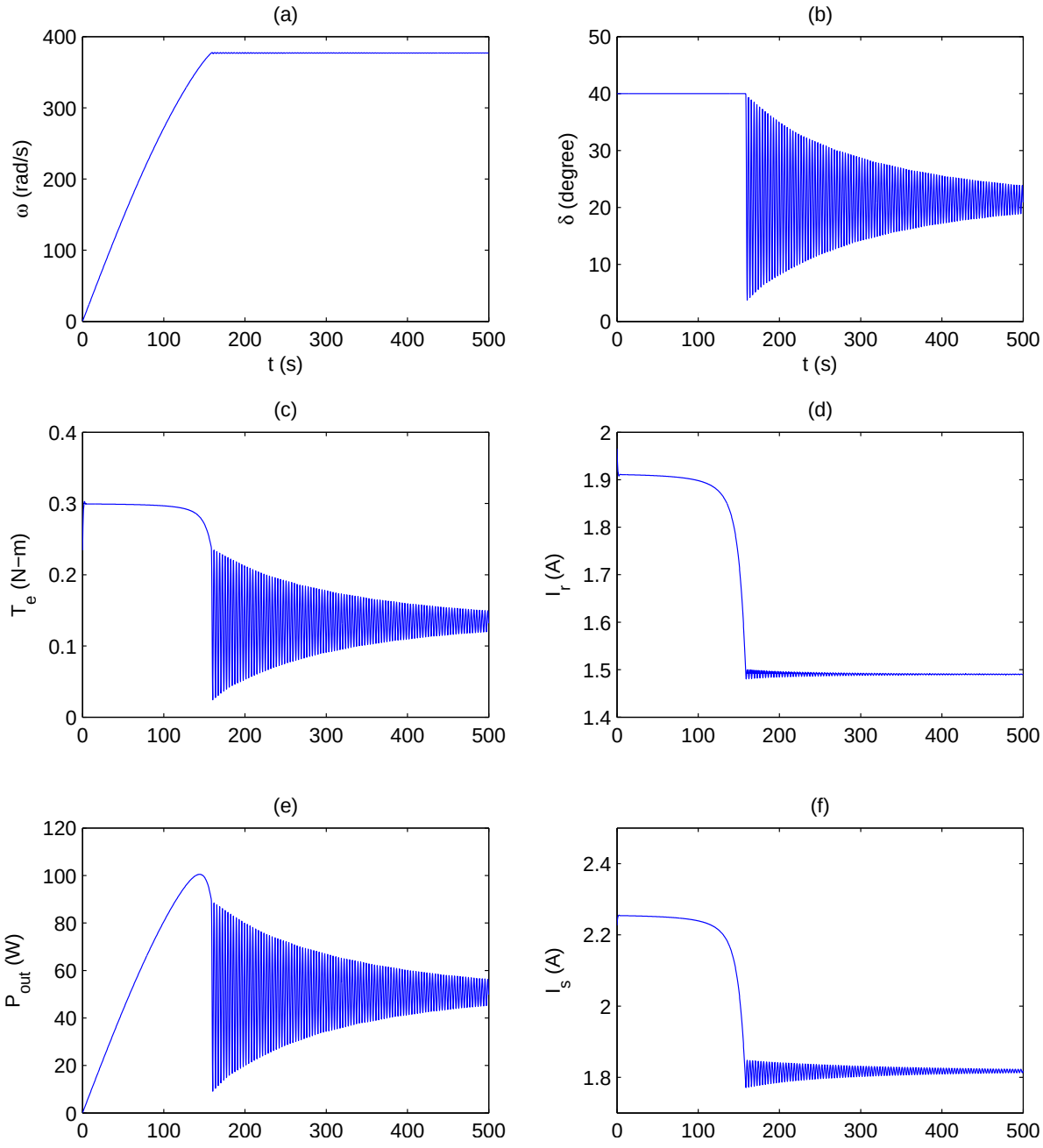

Figure 11: Simulation including eddy currents.

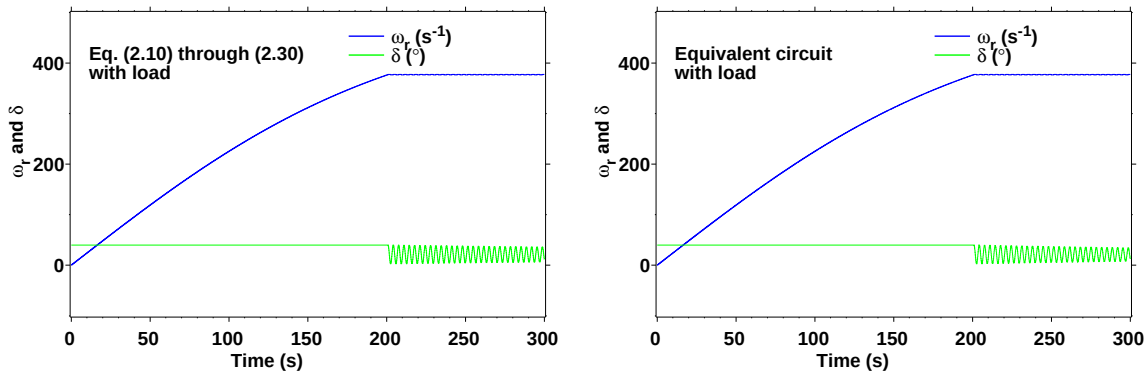

Figure 12: Simulation with non-zero load torque of the full set of equations (left) and the equivalent circuit equations (right).

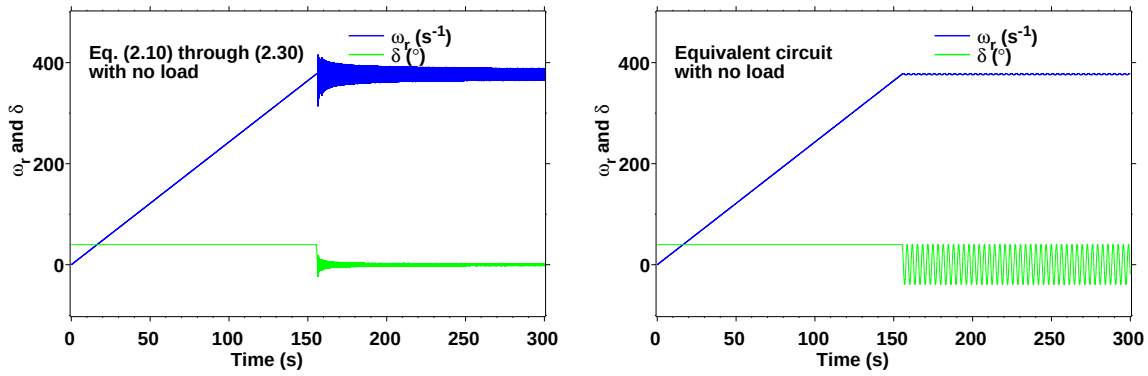

Figure 13: Simulation with no load torque of the full set of equations (left) and the equivalent circuit equations (right).

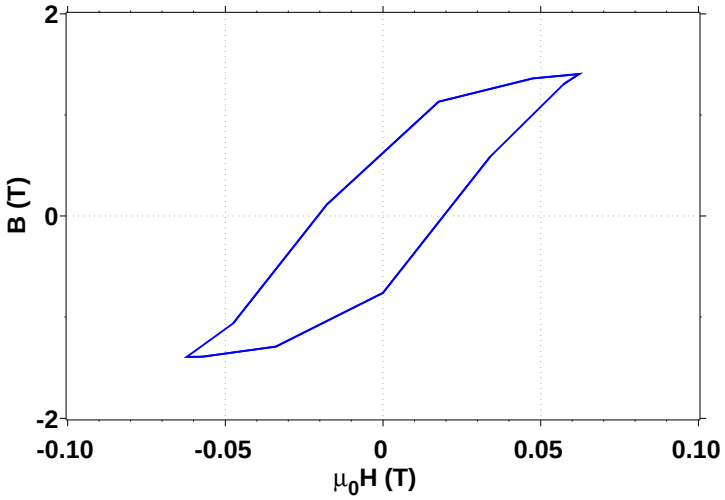

Figure 14: The hysteresis loop, sampled at 11 points.

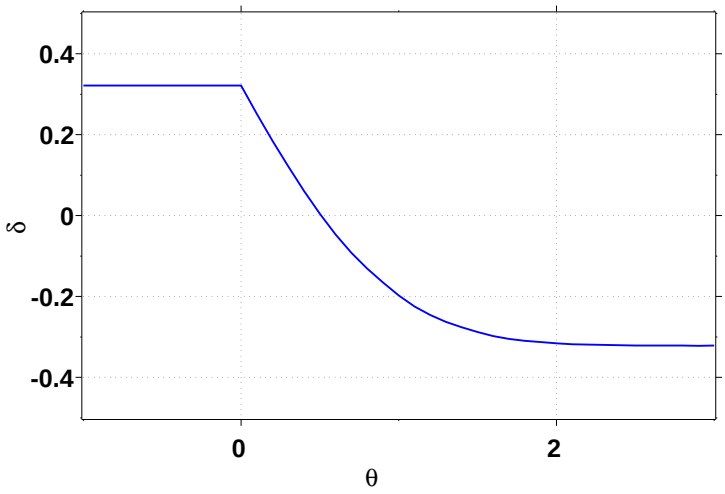

Figure 15: The behavior of the lag angle δ vs rotor angle θ as rotor synchronism is reached and exceeded.

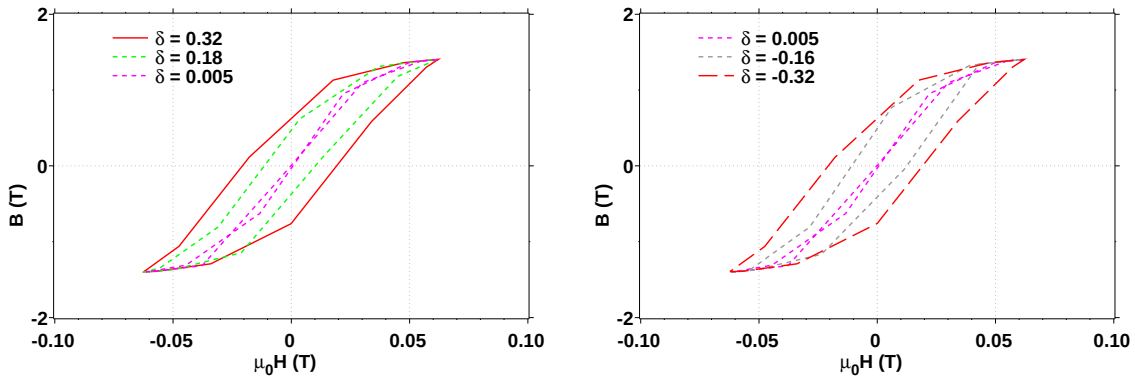

Figure 16: Hysteresis loops at several values of δ, shrinking (left) and re-expanding (right).

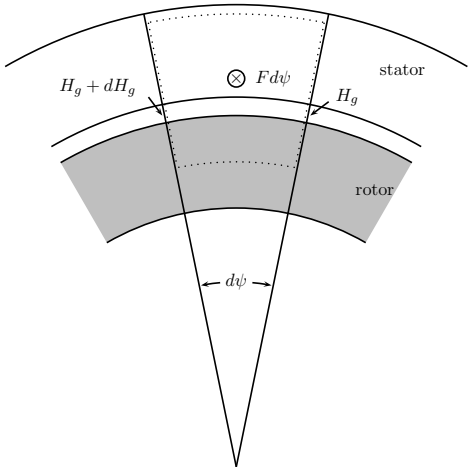

Figure 17: Motor geometry discussed in Miyairi and Kataoka (1965). Eq. (A.1) is developed from integrating H around the dotted loop.

Appendix A

Detailed Derivation of Results in Key Papers

Some of the key papers in the modeling of hysteresis motors are the papers by Miyairi and Kataoka (1965) and Miyairi and Kataoka (1966). Many of the subsequent papers refer to their results. However, a detailed mathematical derivation of their equations is not present. Here, we attempt to remedy the situation. The reader should refer to the papers for the necessary conceptual background information. The motivation and objective of this effort is to (1) check the results, (2) understand the assumptions and limitations, and (3) see if we can extend the work to our needs in any future work, for example, to non-balanced sources.

We have tried to use the same notation as these papers, except for the following differences. We use

1. δ for the lag angle instead of ρ,
2. r_r, r_g instead of R_r, R_g for radii,
3. ℓ_g instead of δ for the air gap width,
4. σ instead of κ for the conductivity,
5. φ_o instead of ψ_o for the phase shift,
6. ω_b instead of ω for the input angular frequency,
7. W instead of Z for the winding factor,
8. N_w instead of W for the number of windings.

A.1 Paper by Miyairi and Kataoka, 1965

A.1.1 Derivation of Apparent Currents

The governing partial differential equations for the B and H fields within the rotor material, as derived by Miyairi and Kataoka, are

$$F = \ell_g \frac{\partial H_g}{\partial \psi} + \frac{r_r}{p} H \ , \tag{A.1}$$

(from Ampere's law, with F the magnetomotive force [current] in a small loop enclosing the rotor material, the air gap, and a small angular section of the stator current; see Fig. 17) and

$$B_g = -\frac{p t_r}{r_g} \frac{\partial B}{\partial \psi} \ , \tag{A.2}$$

(from the divergence equation). Within the air gap, we have

$$B_g = \mu_o H_g \ . \tag{A.3}$$

The variable ψ is the electric angle coordinate in the stator frame.

The B and H field at any particular location in the rotor are assumed to lie on an ellipse of the form:

$$B = B_m \cos\theta, \tag{A.4}$$

$$H = (B_m/\mu)\cos(\theta + \delta), \tag{A.5}$$

where θ is a parametric variable.

The B-field solution is approximated as a sinusoid of the form:

$$B = B_m \cos(\omega_b t - \psi - \varphi_o). \tag{A.6}$$

where φ_o is a phase shift. From (A.5), and setting

$$\theta \equiv \omega_b t - \psi, \tag{A.7}$$

the corresponding expression for the H-field is

$$H = (B_m/\mu)\cos(\omega_b t - \psi - \varphi_o - \delta). \tag{A.8}$$

Substituting (A.6) into (A.2), we have

$$B_g = -\frac{pt_r}{r_g} B_m \sin(\omega_b t - \psi - \varphi_o). \tag{A.9}$$

Substituting this result and (A.8) into (A.1), we have

$$\begin{aligned} F =& \frac{B_m \ell_g p t_r}{\mu_o r_g} \cos(\omega_b t - \psi - \varphi_o) \\ &+ \frac{B_m r_r}{p\mu} \cos(\omega_b t - \psi - \varphi_o + \delta). \end{aligned} \tag{A.10}$$

The conductor density for the k-th phase stator winding is assumed to be of the form

$$W^{(k)} = W \cos(\psi - \psi_k), \tag{A.11}$$

where

$$\psi_k \equiv (k-1)2\pi/m, \tag{A.12}$$

$$W \equiv \frac{2K_w N_w}{p\pi}. \tag{A.13}$$

The balanced current in the k-th phase windings is:

$$I^{(k)} = I \cos(\omega_b t - \psi_k). \tag{A.14}$$

From Appendix C, the resulting magnetomotive force is

$$\begin{aligned} F &= \sum_{k=1}^{m} I^{(k)} W^{(k)} \\ &= \sum_{k=1}^{m} IW \cos(\omega_b t - \psi_k)\cos(\psi - \psi_k) \\ &= \frac{m}{2} IW \cos(\omega_b t - \psi). \end{aligned} \tag{A.15}$$

Eq. (A.10) becomes

$$\begin{aligned} \frac{m}{2} IW \cos(\omega_b t - \psi) = \\ \frac{B_m \ell_g p t_r}{\mu_o r_g} \cos(\omega_b t - \psi - \varphi_o) + \\ \frac{B_m r_r}{p\mu} \cos(\omega_b t - \psi + \delta - \varphi_o). \end{aligned} \tag{A.16}$$

Multiplying both sides by j and replacing ψ by $\psi + \pi/2$ in the above equation, we have

$$\begin{aligned} j\frac{m}{2} IW \sin(\omega_b t - \psi) = \\ j\frac{B_m \ell_g p t_r}{\mu_o r_g} \sin(\omega_b t - \psi - \varphi_o) + \\ j\frac{B_m r_r}{p\mu} \sin(\omega_b t - \psi + \delta - \varphi_o). \end{aligned} \tag{A.17}$$

Adding both sides of this equation to (A.16), we have

$$\begin{aligned} \frac{m}{2} IW e^{j(\omega_b t - \psi)} = \\ \left(\frac{\ell_g p t_r}{\mu_o r_g} + \frac{r_r e^{j\delta}}{p\mu} \right) B_m e^{j(\omega_b t - \psi - \varphi_o)}. \end{aligned} \tag{A.18}$$

Thus, solving for B_m, we have

$$B_m = \frac{mIW}{2} e^{j\varphi_o} \Big/ \left(\frac{\ell_g p t_r}{\mu_o r_g} + \frac{r_r e^{j\delta}}{p\mu} \right). \tag{A.19}$$

Since B_m is a real number, we must have

$$\mathrm{Im}\left\{ e^{j\varphi_o} \left(\frac{\ell_g p t_r}{\mu_o r_g} + \frac{r_r e^{-j\delta}}{p\mu} \right) \right\} = 0. \tag{A.20}$$

The above equation must be satisfied by φ_o. The equation can be shown to be rewritten as

$$\tan\varphi_o = \frac{r_r}{p\mu} \sin\delta \Big/ \left(\frac{\ell_g p t_r}{\mu_o r_g} + \frac{r_r}{p\mu} \cos\delta \right), \tag{A.21}$$

which clearly has a solution for φ_o. Note that φ_o depends on δ.

Thus, we have shown that the fields (A.6) and (A.8) satisfy the partial differential equations (A.1) and (A.2).

It will now be convenient to work in the complex domain. The complex field

$$\mathring{B} = B_m e^{j(\omega_b t - \psi - \varphi_o)} \tag{A.22}$$

gives (A.6) by taking the real part:

$$B = \mathrm{Re}\mathring{B} = B_m \cos(\omega_b t - \psi - \varphi_o). \tag{A.23}$$

From (A.14), the complex current through the k-th phase stator windings is

$$\mathring{I}^{(k)} = I e^{j(\omega_b t - \psi_k)}, \tag{A.24}$$

where, as before, I is a real number. Splitting up both sides up of (A.18) into the individual time-varying components of $e^{j(\omega_b t - \psi_k)}$, we can write

$$\mathring{I}^{(k)} = \mathring{I}_g^{(k)} + \mathring{I}_r^{(k)}, \tag{A.25}$$

where

$$\mathring{I}_g^{(k)} \equiv \frac{2\ell_g p t_r}{m\mu_o r_g W} B_m e^{j(\omega_b t - \psi_k - \varphi_o)}, \tag{A.26}$$

and

$$\mathring{I}_r^{(k)} \equiv \frac{2 r_r e^{j\delta}}{mp\mu W} B_m e^{j(\omega_b t - \psi_k - \varphi_o)}. \tag{A.27}$$

The $\mathring{I}_g^{(k)}$ is the component of the stator current that induces the magnetic field in the air gap. Similarly, the $\mathring{I}_r^{(k)}$ is the component of the stator current that induces the magnetic field within the rotor material.

A.1.2 EMF Derivation

The EMF induced into the k-th phase stator winding by the gap field B_g is is found from application of the Lorentz law:

$$\mathring{\mathcal{E}}_k = -\int_0^{2p\pi} \mathring{B}_g \frac{\omega_b \ell r_g}{p} W \cos(\psi - \psi_k)\, d\psi. \tag{A.28}$$

Note that fluxes emanate from the magnetized poles on the rotor, and that the poles rotate at the angular speed ω_b of the stator field. Thus, the flux lines with intensity B_g are cutting, at a right angle, individual stator conductors of length ℓ at velocity $\omega_b r_g/p$.

From (A.9), we have

$$\mathring{B}_g = j\frac{p t_r B_m}{r_g} e^{j(\omega_b t - \psi - \varphi_o)}. \tag{A.29}$$

Therefore,

$$\begin{aligned}
\mathring{\mathcal{E}}_k = & -j\int_0^{2p\pi} \frac{p t_r B_m}{r_g} e^{j(\omega_b t - \psi - \varphi_o)} \\
& \cdot \frac{\omega_b \ell r_g}{p} W \cos(\psi - \psi_k)\, d\psi \\
= & -j\omega_b t_r B_m \ell W \cdot \\
& \frac{1}{2}\Bigg(\int_0^{2p\pi} e^{j(\omega_b t - \psi_k - \varphi_o)}\, d\psi \\
& + \cancelto{0}{\int_0^{2p\pi} e^{j(\omega_b t - 2\psi + \psi_k - \varphi_o)}\, d\psi} \Bigg) \\
= & -j\pi p \omega_b t_r \ell W B_m e^{j(\omega_b t - \psi_k - \varphi_o)}.
\end{aligned} \tag{A.30}$$

A.1.3 Impedances

From (A.26) and (A.30), the apparent impedance for the air gap is

$$\begin{aligned}
\mathring{Z}_g &= \frac{-\mathring{\mathcal{E}}_k}{\mathring{I}_g^{(k)}} \\
&= \frac{j\omega_b \pi t_r \ell W p}{2\ell_g p t_r / m\mu_o r_g W} \\
&= j\frac{\omega_b \pi \ell r_g W^2 m \mu_o}{2\ell_g} \\
&= j\frac{2\omega_b \ell r_g K_w^2 N_w^2 m \mu_o}{p^2 \pi \ell_g}.
\end{aligned} \tag{A.31}$$

This corresponds to an inductance:

$$L_m = \frac{2\ell r_g K_w^2 N_w^2 m \mu_o}{p^2 \pi \ell_g}. \tag{A.32}$$

From (A.27) and (A.30), the apparent

impedance in the rotor material is

$$\begin{aligned}\mathring{Z}_r &= \frac{-\mathring{\mathcal{E}}_k}{\mathring{I}_r^{(k)}} \\ &= \frac{j\omega_b \pi t_r \ell W p}{2r_r e^{j\delta}/mp\mu W} \\ &= j\frac{\omega_b \pi t_r \ell W^2 p^2 m\mu}{2r_r e^{j\delta}} \\ &= j\frac{2\omega_b t_r \ell K_w^2 N_w^2 m\mu}{r_r \pi} e^{-j\delta}. \end{aligned} \tag{A.33}$$

This corresponds to a resistance:

$$R_r = \frac{2\omega_b t_r \ell K_w^2 N_w^2 m\mu}{r_r \pi} \sin\delta, \tag{A.34}$$

and inductance:

$$L_{hr} = \frac{2t_r \ell K_w^2 N_w^2 m\mu}{r_r \pi} \cos\delta, \tag{A.35}$$

that are connected in series. Note that the resistance increases with frequency.

From Eq. (A.25), note that the impedances correspond to an equivalent circuit with parallel impedances $\mathring{Z}_g$ and $\mathring{Z}_r$.

A.2 Paper by Miyairi and Kataoka, 1966

This paper extended their previous work by including the effect of eddy currents in the rotor for the case of a circumferential-flux motor.

A.2.1 Magnetic Field Solution

In what follows the B and H field will be complex, unless otherwise noted. Neglecting edge effects, we only consider the field dependence in the angular and radial coordinate directions. The B-field is assumed to be of the form:

$$\mathbf{B}(x,y,t) = \mathbf{R}(r) e^{j(s\omega_b t - \psi_r - \varphi_o)}, \tag{A.36}$$

where

$$s \equiv (\omega_b - \omega_r)/\omega_b \tag{A.37}$$

is the slip, and ψ_r is the electric angular coordinate. From the elliptical hysteresis curve assumption, we have from (A.5) that

$$\mathbf{H}(x,y,t) = \mathbf{R}(r)\frac{1}{\mu} e^{j(s\omega_b t - \psi_r + \delta - \varphi_o)}. \tag{A.38}$$

The relationship between the two fields may be written as

$$\mathbf{B} = \mathring{\mu}\mathbf{H}, \tag{A.39}$$

where we define the complex magnetic permeability by

$$\mathring{\mu} \equiv \mu e^{-j\delta}. \tag{A.40}$$

Maxwell's Equations are

$$\nabla \times \mathbf{E} = -\frac{\partial \mathbf{B}}{\partial t}, \tag{A.41}$$

$$\nabla \times \mathbf{H} = \mathbf{I} - \frac{\partial \mathbf{D}}{\partial t}, \tag{A.42}$$

$$\nabla \cdot \mathbf{D} = \rho, \tag{A.43}$$

$$\nabla \cdot \mathbf{B} = 0. \tag{A.44}$$

The constituitive relation

$$\mathbf{I} = \sigma \mathbf{E}. \tag{A.45}$$

is needed to close the equations.

In the rotor material, we assume (1) no charges, (2) no dielectric properties, and (3) neglect displacement currents. Then, $\rho = 0$ and $\mathbf{D} = \epsilon_o \mathbf{E}$. Eqs. (A.42) and (A.43) reduce to

$$\nabla \times \mathbf{H} = \mathbf{I}, \tag{A.46}$$

$$\nabla \cdot \mathbf{E} = 0. \tag{A.47}$$

From (A.39) and (A.44), we have

$$\nabla \cdot \mathbf{H} = 0. \tag{A.48}$$

Taking the curl of (A.42) and using the general vector identity:

$$\nabla \times \nabla \times \mathbf{F} = \nabla(\nabla \cdot \mathbf{F}) - \nabla^2 \mathbf{F}, \tag{A.49}$$

we have

$$\begin{aligned} -\nabla^2 \mathbf{H} &= \nabla \times \mathbf{I} \\ &= \sigma \nabla \times \mathbf{E}. \end{aligned} \tag{A.50}$$

From (A.41) we have

$$\nabla^2 \mathbf{H} = \sigma \frac{\partial \mathbf{B}}{\partial t}. \tag{A.51}$$

From (A.39) we have

$$\nabla^2 \mathbf{B} = \mathring{\mu}\sigma \frac{\partial \mathbf{B}}{\partial t}. \tag{A.52}$$

We will assume that the radius of the rotor is sufficiently large that its shape can be approximated as a periodic rectangular region. Consequently, we use the coordinate transformation

$$\psi_r = \pi x/\tau, \tag{A.53}$$

where x is the rectilinear coordinate and τ is the pole pitch:

$$\tau \equiv \pi r_s/p, \tag{A.54}$$

with r_s denoting the stator radius at the air gap.

The coordinate y will be associated with the radial direction r, and z will be the coordinate in the axial direction.

The required boundary conditions on the B-field are

$$(B_x)_{x=0} = (B_x)_{x=2\tau}, \tag{A.55}$$

$$(B_y)_{y=0} = 0, \tag{A.56}$$

$$(B_y)_{y=t_r} = \frac{B_{gm}}{\sqrt{2}} e^{j(s\omega_b t - \pi x/\tau - \varphi_o)}. \tag{A.57}$$

where

Neglecting edge effects, for all z, we have

$$B_z = 0. \tag{A.58}$$

We assume a solution of the form:

$$\mathbf{B}(x, y, t) = \mathbf{Y}(y) e^{j(s\omega_b t - \pi x/\tau - \varphi_o)}, \tag{A.59}$$

which meets the x-periodic boundary condition (A.55). Substituting into (A.52), we have

$$\frac{\partial^2 \mathbf{Y}}{\partial y} - \left(\frac{\pi}{\tau}\right)^2 \mathbf{Y} = j\mathring{\mu}\sigma s\omega_b \mathbf{Y}. \tag{A.60}$$

Or,

$$\frac{\partial^2 \mathbf{Y}}{\partial y} - \left[\left(\frac{\pi}{\tau}\right)^2 + j\mathring{\mu}\sigma s\omega_b\right] \mathbf{Y} = 0. \tag{A.61}$$

Define

$$\begin{aligned} c &= t_r \sqrt{\left(\frac{\pi}{\tau}\right)^2 + j\mathring{\mu}\sigma s\omega_b} \\ &= t_r \sqrt{\left(\frac{\pi}{\tau}\right)^2 + j(\cos\delta - j\sin\delta)\sigma s\omega_b \mu} \\ &= t_r \sqrt{\left(\left(\frac{\pi}{\tau}\right)^2 + \sigma s\omega_b \mu \sin\delta\right) + j\sigma s\omega_b \mu \cos\delta}. \end{aligned} \tag{A.62}$$

Then,

$$\frac{\partial^2 \mathbf{Y}}{\partial y^2} - \left(\frac{c}{t_r}\right)^2 \mathbf{Y} = 0. \tag{A.63}$$

From the boundary conditions we have

$$Y_y = \frac{B_{gm}}{\sqrt{2}} \frac{\sinh(cy/t_r)}{\sinh(c)}. \tag{A.64}$$

From (A.44), we have

$$\frac{\partial B_x}{\partial x} + \frac{\partial B_y}{\partial y} = 0, \tag{A.65}$$

which from the form of our solution implies

$$-\frac{j\pi}{\tau} Y_x + \frac{\partial Y_y}{\partial y} = 0. \tag{A.66}$$

Thus,

$$Y_x = -j\frac{\tau}{\pi}\frac{\partial Y_y}{\partial y} \tag{A.67}$$

$$= -j\frac{B_{gm}}{\sqrt{2}}\frac{\tau}{\pi}\frac{c}{t_r}\frac{\cosh(cy/t_r)}{\sinh(c)}. \tag{A.68}$$

Summarizing, the magnetic field components are

$$B_x = -j\frac{B_{gm}}{\sqrt{2}}\frac{\tau}{\pi}\frac{c}{t_r}\frac{\cosh(cy/t_r)}{\sinh(c)} e^{j(s\omega_b t - \pi x/\tau - \varphi_o)}, \tag{A.69}$$

and

$$B_y = \frac{B_{gm}}{\sqrt{2}}\frac{\sinh(cy/t_r)}{\sinh(c)} e^{j(s\omega_b t - \pi x/\tau - \varphi_o)}). \tag{A.70}$$

Expressions for c

We now derive some expressions for c that we need to use later. We define the quantities:

$$\alpha \equiv \mathrm{Re}(c), \qquad \beta \equiv \mathrm{Im}(c), \tag{A.71}$$

so that

$$c = \alpha + j\beta. \tag{A.72}$$

Given any complex $u + jv$, it can be shown that

$$\sqrt{u+vj} = \sqrt{\frac{1}{2}(r+u)} + j\,\mathrm{sgn}(v)\cdot\sqrt{\frac{1}{2}(r-u)}, \tag{A.73}$$

where $r \equiv \sqrt{u^2+v^2}$. Thus, from (A.62), we have

$$\alpha = \sqrt{\frac{1}{2}(\gamma+\eta)}, \tag{A.74}$$

$$\beta = \mathrm{sgn}(s\cos\delta)\sqrt{\frac{1}{2}(\gamma-\eta)}, \tag{A.75}$$

where we define the following:

$$\gamma \equiv t_r^2\sqrt{\left(\frac{\pi}{\tau}\right)^4 + 2\left(\frac{\pi}{\tau}\right)^2\sigma s\omega_b\mu\sin\delta + (\sigma s\omega_b\mu)^2}, \tag{A.76}$$

$$\eta \equiv t_r^2\cdot\left[\left(\frac{\pi}{\tau}\right)^2 + \sigma s\omega_b\mu\sin\delta\right]. \tag{A.77}$$

From the above, note that the following identity holds:

$$\alpha^2 - \beta^2 = \eta. \tag{A.78}$$

Thus,

$$\alpha^2 + \beta^2 = -\eta + 2\alpha^2, \tag{A.79}$$

and

$$\alpha^2 + \beta^2 = \eta + 2\beta^2. \tag{A.80}$$

Another expression, resulting directly from (A.74) and (A.75), is

$$\begin{aligned} 2\alpha\beta &= \mathrm{sgn}(s\cos\delta)\sqrt{\gamma^2-\eta^2} \\ &= t_r^2\sigma s\omega_b\mu\cos\delta. \end{aligned} \tag{A.81}$$

A.2.2 Equivalent Circuit

The stator has m pairs of input leads where m is the number of phases. The stator consists of p pole pairs. There are $2p$ stator coils (one for each pole) with each coil connected to a single particular phase. The particular phases of a coil alternate in consecutive order as we go around the stator.

We wish to find an equivalent circuit that will duplicate the current-voltage relationship as seen by the input to the windings of each phase. The equivalent circuit must include stator coils and the electromagnetic interaction of the rotor with the stator coils; in particular, the back-EMF from the rotor magnetic field. In this section, we first neglect mutual inductance between stator coils. This effect can be added to the equivalent circuit through additional inductances, as shown in the main text of this report.

As is commonly done, the stator is assumed to have symmetrical perfect m-phase windings with conductor density (no. of conductors/radian) for the k-th phase given by

$$W_{(k)} = W\cos(\pi x'/\tau - \psi_k), \tag{A.82}$$

$$k = 1, 2, ..., m. \tag{A.83}$$

Here, W is the maximum conductor density given by

$$W = 2K_w N_w/p\pi, \tag{A.84}$$

where N_w is the number of stator coil windings per phase and K_w is the winding coefficient ($0 < K_w \leq 1$). The phase shift ψ_k is defined as

$$\psi_k \equiv \frac{(k-1)2\pi}{m}, \qquad k = 1, ..., m. \tag{A.85}$$

By using Ampere's circuit law, from Miyairi and Kataoka (1966) we obtain the equation relating the air gap field and rotor edge field:

$$F = \frac{\tau\ell_g}{\pi}\frac{\partial H_g}{\partial x} + \frac{\tau}{\pi}(H_x)_{y=t_r}. \tag{A.86}$$

Here, ℓ_g is the air gap thickness, and F is the magnetomotive force produced by the stator field. The

gap field H_g is given by

$$H_g = (B_y)_{y=t_r}/\mu_o. \tag{A.87}$$

And within the rotor, at the air gap interface, we have

$$(H_x)_{t=t_r} = (B_x)_{t=t_r}/\mathring{\mu}. \tag{A.88}$$

Thus, (A.86) becomes

$$F = \frac{\tau \ell_g}{\pi \mu_o}\frac{\partial (B_y)_{y=t_r}}{\partial x} + \frac{\tau}{\pi \mathring{\mu}}(B_x)_{y=t_r}. \tag{A.89}$$

Assuming that

$$I^{(k)} = Ie^{j(\omega_b t - \psi_k)}, \tag{A.90}$$

where I is real, we show in Appendix C that the complex magnetomotive force can be written as

$$F = \frac{m}{2} IW e^{j(\omega_b t - \pi x'/\tau)}, \tag{A.91}$$

where x' is the variable corresponding to x in the stationary stator frame.

Substituting (A.69), (A.70), (A.91) into (A.86), we have

$$\begin{aligned}\frac{m}{2}IWe^{j(\omega_b t-\pi x'/\tau)} = \\ \frac{\ell_g B_{gm}}{\mu_o\sqrt{2}}e^{j(s\omega_b t-\pi x/\tau-\varphi_o)} \\ + \frac{\tau^2 B_{gm} c}{\pi^2 \mathring{\mu} t_r \sqrt{2}}\coth(c)e^{j(s\omega_b t-\pi x/\tau-\varphi_o)}.\end{aligned} \tag{A.92}$$

From

$$x' = x - \omega_r t\tau/\pi = x - (1-s)\omega_b t\tau/\pi, \tag{A.93}$$

we have that

$$\begin{aligned}s\omega_b t - \pi x/\tau &= s\omega_b t - \pi x'\tau/pi + (1-s)\omega_b t \\ &= \omega_b t - \pi x'\tau/\pi.\end{aligned} \tag{A.94}$$

Therefore, (A.92) becomes

$$\begin{aligned}\frac{m}{2}IWe^{j(\omega_b t-\pi x'/\tau)} = -j\frac{\ell_g B_{gm}}{\mu_o\sqrt{2}}e^{j(\omega_b t-\pi x'/\tau-\varphi_o)} \\ - j\frac{\tau^2 B_{gm} c}{\pi^2 \mathring{\mu} t_r \sqrt{2}}\coth(c)e^{j(\omega_b t-\pi x'/\tau-\varphi_o)}.\end{aligned} \tag{A.95}$$

Solving for I, we have

$$I = -j\frac{2e^{-j\varphi_o}}{mW}\left(\frac{\ell_g B_{gm}}{\mu_o\sqrt{2}} + \frac{\tau^2 B_{gm} c}{\pi^2 \mathring{\mu} t_r \sqrt{2}}\coth(c)\right). \tag{A.96}$$

The phase shift φ_o is selected such that the imaginary part of the above expression is zero so that the expression will be a real number.

Multiplying both sides of this equation by $e^{j(\omega_b t-\psi_k)}$ we have

$$\begin{aligned}Ie^{j(\omega_b t-\psi_k)} = & -j\frac{2}{mW}\left(\frac{\ell_g B_{gm}}{\mu_o\sqrt{2}}e^{j(\omega_b t-\psi_k-\varphi_o)}\right. \\ & \left. + \frac{\tau^2 B_{gm} c}{\pi^2 \mathring{\mu} t_r \sqrt{2}}\coth(c)e^{j(\omega_b t-\psi_k-\varphi_o)}\right).\end{aligned} \tag{A.97}$$

Thus, we have

$$I^{(k)} = I_g^{(k)} + I_r^{(k)}, \tag{A.98}$$

where

$$I_g^{(k)} \equiv -j\frac{2\ell_g B_{gm}}{\mu_o mW\sqrt{2}}e^{j(\omega_b t-\psi_k-\varphi_o)}, \tag{A.99}$$

and

$$I_r^{(k)} \equiv -j\frac{2\tau^2 B_{gm} c}{\pi^2 \mathring{\mu} t_r mW\sqrt{2}}\coth(c)e^{j(\omega_b t-\psi_k-\varphi_o)}. \tag{A.100}$$

For phase k, the current $I_g^{(k)}$ may viewed as the "air gap current" and $I_r^{(k)}$ as the "rotor current", although the latter is not a true current in the rotor but rather one component of the stator current.

Induced EMF through Coils of a Single Phase

Let B_s denote the corresponding component of the B-field through this interface. We make the approximation that the flux lines between the rotor and stator in the air gap are perpendicular to the rotor and stator surfaces so that B_s is the equal to $B_{y=t_r}$, but translated in the x direction because the

rotor is rotating relative to the stator. The coordinate x' on the stator is related to the x coordinate on the rotor through

$$x' = x - \omega_r t\tau/\pi = x - (1-s)\omega_b t\tau/\pi. \quad \text{(A.101)}$$

Thus, from (A.57), we have

$$\begin{aligned}(B_s)_{x'} &= (B_y)_{x=x'+\omega_b(1-s)t\tau/\pi, y=t_r} \\ &= \frac{B_{gm}}{\sqrt{2}} e^{j(\omega_b t - \pi x'/\tau)}. \end{aligned} \quad \text{(A.102)}$$

From the Lorentz law, the electromotive force is

$$\mathcal{E}^{(k)} = -\ell\omega_b \int_0^{2\pi} B_s W^{(k)} d\theta, \quad \text{(A.103)}$$

where θ is the physical angle around the rotor, which is related to x' by

$$\theta = \pi x'/p\tau. \quad \text{(A.104)}$$

From (A.102) and (A.83), we have

$$\begin{aligned}\mathcal{E}^{(k)} = & -\ell\omega_b \int_0^{2\tau} \frac{B_{gm}}{\sqrt{2}} e^{j(\omega_b t - \pi x'/\tau)} \\ & \cdot W\cos(\pi x'/\tau - (k-1)2\pi/m)\left(\frac{\pi}{p\tau}dx'\right) \\ = & -\frac{\ell\omega_b B_{gm}\pi W}{\sqrt{2}p\tau} e^{j\omega_b t}\int_0^{2p\tau} e^{-j\pi x'/\tau} \\ & \cdot \left(\frac{1}{2}e^{j\pi x'/\tau - j(k-1)2\pi/m} \right. \\ & \left. + \frac{1}{2}e^{-j\pi x'/\tau + j(k-1)2\pi/m}\right)dx'. \end{aligned} \quad \text{(A.105)}$$

By algebraic manipulation, we have

$$\begin{aligned}\mathcal{E}^{(k)} = & -\frac{\ell\omega_b B_{gm}\pi W}{\sqrt{2}p\tau} e^{j\omega_b t}\cdot\left(\frac{1}{2}e^{-j(k-1)2\pi/m}\int_0^{2p\tau} dx' \right. \\ & \left. + \frac{1}{2}\int_0^{2p\tau} e^{-2j\pi x'/\tau + j(k-1)2\pi/m}dx'\right) \\ = & -\frac{\ell\omega_b B_{gm}\pi W}{\sqrt{2}p\tau} e^{j\omega_b t}\cdot\left(p\tau e^{-j(k-1)2\pi/m} \right. \\ & \left. + \frac{\tau}{-4\pi j}e^{j(k-1)2\pi/m}\left[e^{-2j\pi x'/\tau}\right]_0^{2p\tau}\right)dx' \\ = & -\frac{\ell\omega_b B_{gm}\pi W}{\sqrt{2}p\tau} e^{j\omega_b t}\cdot\left(p\tau e^{-j(k-1)2\pi/m} \right. \\ & \left. + \frac{\tau}{-4\pi j}e^{j(k-1)2\pi/m}\cancelto{0}{\left(e^{-4\pi pj}-1\right)}\right)dx' \\ = & -\frac{\ell\omega_b B_{gm}\pi W}{\sqrt{2}} e^{j(\omega_b t - (k-1)2\pi/m)}. \end{aligned} \quad \text{(A.106)}$$

Apparent Impedances

The apparent impedance of the k-th phase circuit is given by

$$Z^{(k)} \equiv \frac{-\mathcal{E}^{(k)}}{I^{(k)}}. \quad \text{(A.107)}$$

The individual impedances of the gap and rotor currents are

$$\begin{aligned} Z_g \equiv Z_g^{(k)} &\equiv \frac{-\mathcal{E}^{(k)}}{I_g^{(k)}} \\ &= j\omega_b \frac{\ell\pi\mu_o W^2}{\ell_g} \\ &= j\omega_b \frac{4\ell\mu_o K_w^2 N_w^2}{\ell_g p^2 \pi}. \end{aligned} \quad \text{(A.108)}$$

and

$$\begin{aligned} Z_r \equiv Z_r^{(k)} &\equiv \frac{-\mathcal{E}^{(k)}}{I_r^{(k)}} \\ &= j\omega_b \frac{\ell\pi^3 \mathring{\mu} t_r W^2 m \tanh(c)}{2\tau^2 c} \\ &= j\omega_b \frac{2\ell\mathring{\mu} t_r K_w^2 N_w^2 m \tanh(c)}{\tau^2 p^2 c}. \end{aligned} \quad \text{(A.109)}$$

Real and Imaginary Parts of Z_r

We now find expressions for the real and imaginary parts of Z_r. We have

$$Z_r = h\frac{je^{-j\delta}\tanh(c)}{c}, \tag{A.110}$$

where

$$h \equiv \frac{2m\omega_b\mu\ell t_r K_w^2 N_w^2}{\tau^2 p^2}. \tag{A.111}$$

We first derive some hyperbolic trignometric indentities. From the identities:

$$\sinh(c+c^*) = \sinh(c)\cosh(c^*) + \cosh(c)\sinh(c^*),$$

$$\sinh(c-c^*) = \sinh(c)\cosh(c^*) - \cosh(c)\sinh(c^*),$$

we have that

$$\sinh(c+c^*) + \sinh(c-c^*) = 2\sinh(c)\cosh(c^*),$$

which implies that

$$\begin{aligned}\sinh(2\alpha) + j\sin(2\beta) &= 2\sinh(c)\cosh(c^*)\\ &= 2\tanh(c)\cosh(c)\cosh(c^*)\end{aligned} \tag{A.112}$$

And from the identities:

$$\cosh(c+c^*) = \sinh(c)\sinh(c^*) + \cosh(c)\cosh(c^*),$$

$$\cosh(c-c^*) = -\sinh(c)\sinh(c^*) + \cosh(c)\cosh(c^*),$$

we have that

$$\cosh(c+c^*) + \cosh(c-c^*) = 2\cosh(c)\cosh(c^*),$$

which implies that

$$\cosh(2\alpha) + \cos(2\beta) = 2\cosh(c)\cosh(c^*). \tag{A.113}$$

Therefore, we have

$$\tanh(c) = \frac{\sinh(2\alpha) + j\sin(2\beta)}{\cosh(2\alpha) + \cos(2\beta)}. \tag{A.114}$$

Thus,

$$\begin{aligned}Z_r &= h\frac{je^{-j\delta}\tanh(c)}{c}\\ &= h\frac{je^{-j\delta}c^*\tanh(c)}{|c|^2}\\ &= h\tanh(c)\frac{(\sin\delta + j\cos\delta)(\alpha - j\beta)}{\alpha^2+\beta^2}\\ &= h\tanh(c)\cos\delta\frac{(\tan\delta + j)(\alpha - j\beta)}{\alpha^2+\beta^2}\\ &= h\tanh(c)\cos\delta\frac{(\alpha\tan\delta + \beta) + j(\alpha - \beta\tan\delta)}{\alpha^2+\beta^2}\\ &= h\cos\delta\frac{(\alpha\tan\delta + \beta) + j(\alpha - \beta\tan\delta)}{\alpha^2+\beta^2}\\ &\quad\cdot\frac{\sinh 2\alpha + j\sin 2\beta}{\cosh 2\alpha + \cos 2\beta}.\end{aligned} \tag{A.115}$$

Hence,

$$\begin{aligned}\mathrm{Re}Z_r = \frac{h}{(\alpha^2+\beta^2)(\cosh 2\alpha + \cos 2\beta)}\\ \cdot\Big[(\alpha\sinh 2\alpha + \beta\sin 2\beta)\sin\delta\\ + (\beta\sinh 2\alpha - \alpha\sin 2\beta)\cos\delta\Big]\end{aligned} \tag{A.116}$$

and

$$\begin{aligned}\mathrm{Im}Z_r = \frac{h}{(\alpha^2+\beta^2)(\cosh 2\alpha + \cos 2\beta)}\\ \cdot\Big[(-\beta\sinh 2\alpha + \alpha\sin 2\beta)\sin\delta\\ + (\alpha\sinh 2\alpha + \beta\sin 2\beta)\cos\delta\Big].\end{aligned} \tag{A.117}$$

A.2.3 Hysteresis Force Derivation

We now compute the force from hysteresis:

$$\begin{aligned}F_H = p\ell\int_0^{t_r}\int_0^{2\tau}\Big(&\mathrm{Re}B_x\frac{\partial\mathrm{Re}H_x}{\partial x}\\ &+\mathrm{Re}B_y\frac{\partial\mathrm{Re}H_y}{\partial x}\Big)\,dxdy,\end{aligned} \tag{A.118}$$

where p is the number of pole pairs.

We have the identity:

$$\begin{aligned}\mathrm{Re}(a)\mathrm{Re}(b) &= \frac{1}{4}(a+a^*)(b+b^*) \\ &= \frac{1}{4}(ab+a^*b^*+a^*b+ab^*) \quad \text{(A.119)} \\ &= \frac{1}{2}[\mathrm{Re}(ab)+\mathrm{Re}(a^*b)]. \quad \text{(A.120)}\end{aligned}$$

Each term in the integral is of the form:

$$\begin{aligned}\mathrm{Re}B_u\frac{\partial \mathrm{Re}H_u}{\partial x} =& \mathrm{Re}(B_u)\mathrm{Re}\left(\frac{\partial H_u}{\partial x}\right) \\ =& \frac{1}{2}\mathrm{Re}\left(B_u\frac{\partial H_u}{\partial x}\right)+ \\ & \frac{1}{2}\mathrm{Re}\left(B_u^*\frac{\partial H_u}{\partial x}\right), \quad \text{(A.121)} \\ u = x, y.&\end{aligned}$$

From (A.39) we have

$$\begin{aligned}\mathrm{Re}B_u\frac{\partial \mathrm{Re}H_u}{\partial x} =& \frac{1}{2}\mathrm{Re}\left(\frac{B_u}{\mathring{\mu}}\frac{\partial B_u}{\partial x}\right)+ \\ & \frac{1}{2}\mathrm{Re}\left(\frac{B_u^*}{\mathring{\mu}}\frac{\partial B_u}{\partial x}\right). \quad \text{(A.122)}\end{aligned}$$

From (A.59), we have

$$\begin{aligned}&\mathrm{Re}B_u\frac{\partial \mathrm{Re}H_u}{\partial x} = \\ &\frac{1}{2}\mathrm{Re}\left(\frac{Y_u^2}{\mathring{\mu}}\cdot\frac{-j\pi}{\tau}e^{2j(s\omega_b t-\pi x/\tau)}\right)+ \\ &\frac{1}{2}\mathrm{Re}\left(\frac{|Y_u|^2}{\mathring{\mu}}\cdot\frac{-j\pi}{\tau}\right). \quad \text{(A.123)}\end{aligned}$$

Upon integrating w.r.t. x, we have that the first term vanishes because

$$\begin{aligned}\int_0^{2\tau} e^{2j(s\omega_b t-\pi x/\tau)}dx &= \frac{\tau}{\pi}\left[e^{2j(s\omega_b t-\pi x/\tau)}\right]_0^{2\tau} \\ &= \frac{\tau}{\pi}e^{2js\omega_b t}\left[e^{-4\pi j}-1\right] \\ &= \frac{\tau}{\pi}e^{2js\omega_b t}\left[\cos 4\pi - 1\right] \\ &= 0. \quad \text{(A.124)}\end{aligned}$$

Therefore,

$$\begin{aligned}&\int_0^{t_r}\int_0^{2\tau}\mathrm{Re}B_u\frac{\partial \mathrm{Re}H_u}{\partial x}dxdy \\ &= \int_0^{t_r}\frac{1}{2}\mathrm{Re}\left(\frac{|Y_u|^2}{\mathring{\mu}}\cdot\frac{-j\pi}{\tau}\right)\cdot 2\tau\, dy \\ &= \frac{\pi}{\mu}\int_0^{t_r}|Y_u|^2\mathrm{Re}\left(-j\cos\delta+\sin\delta\right)dy \\ &= \frac{\pi\sin\delta}{\mu}\int_0^{t_r}|Y_u|^2dy. \quad \text{(A.125)}\end{aligned}$$

From (A.67), we have that

$$|Y_x|^2 = \frac{B_{gm}^2}{2}\left(\frac{\tau}{\pi t_r}\right)^2\frac{|c|^2\,|\cosh(cy/t_r)|^2}{|\sinh(c)|^2}, \quad \text{(A.126)}$$

and, from (A.64), we have

$$|Y_y|^2 = \frac{B_{gm}^2}{2}\frac{|\sinh(cy/t_r)|^2}{|\sinh(c)|^2}. \quad \text{(A.127)}$$

From the definition of hyperbolic functions, we have that

$$\begin{aligned}|\cosh\zeta|^2 &= \cosh\zeta\cosh\zeta^* \\ &= \frac{1}{4}(e^{\zeta}+e^{-\zeta})(e^{\zeta^*}+e^{-\zeta^*}) \\ &= \frac{1}{4}(e^{\zeta+\zeta^*}+e^{\zeta-\zeta^*}+e^{-\zeta+\zeta^*}+e^{-\zeta-\zeta^*}) \\ &= \frac{1}{4}\Big(e^{2\mathrm{Re}(\zeta)}+e^{2j\mathrm{Im}(\zeta)} \\ &\quad +e^{-2j\mathrm{Im}(\zeta)}+e^{-2\mathrm{Re}(\zeta)}\Big) \\ &= \frac{1}{2}\left[\cosh(2\mathrm{Re}(\zeta))+\cos(2\mathrm{Im}(\zeta))\right]. \quad \text{(A.128)}\end{aligned}$$

Similarly, we have

$$\begin{aligned}|\sinh\zeta|^2 &= \sinh\zeta\sinh\zeta^* \\ &= \frac{1}{4}(e^{\zeta}-e^{-\zeta})(e^{\zeta^*}-e^{-\zeta^*}) \\ &= \frac{1}{4}(e^{\zeta+\zeta^*}-e^{\zeta-\zeta^*}-e^{-\zeta+\zeta^*}+e^{-\zeta-\zeta^*}) \\ &= \frac{1}{4}\Big(e^{2\mathrm{Re}(\zeta)}-e^{2j\mathrm{Im}(\zeta)} \\ &\quad -e^{-2j\mathrm{Im}(\zeta)}+e^{-2\mathrm{Re}(\zeta)}\Big) \\ &= \frac{1}{2}\left[\cosh(2\mathrm{Re}(\zeta))-\cos(2\mathrm{Im}(\zeta))\right]. \quad \text{(A.129)}\end{aligned}$$

Therefore, (A.126) and (A.127) become

$$|Y_x|^2 = \frac{B_{gm}^2}{2}\left(\frac{\tau}{\pi t_r}\right)^2(\alpha^2+\beta^2) \cdot \frac{\cosh(2\alpha y/t_r)+\cos(2\beta y/t_r)}{\cosh 2\alpha - \cos 2\beta}, \quad \text{(A.130)}$$

$$|Y_y|^2 = \frac{B_{gm}^2}{2}\frac{\cosh(2\alpha y/t_r)-\cos(2\beta y/t_r)}{\cosh 2\alpha - \cos 2\beta}. \quad \text{(A.131)}$$

We now integrate w.r.t. y, to give

$$\int_0^{t_r}|Y_x|^2 dy = \frac{B_{gm}^2}{2}\left(\frac{\tau}{\pi t_r}\right)^2(\alpha^2+\beta^2) \cdot \frac{(t_r/2\alpha)\sinh 2\alpha + (t_r/2\beta)\sin 2\beta}{\cosh 2\alpha - \cos 2\beta}. \quad \text{(A.132)}$$

From (A.79) and (A.80), we have

$$\int_0^{t_r}|Y_x|^2 dy = \frac{B_{gm}^2}{2t_r}\left(\frac{\tau}{\pi}\right)^2 \cdot \frac{(-\frac{\eta}{\alpha}+2\alpha)\sinh 2\alpha + (\frac{\eta}{\beta}+2\beta)\sin 2\beta}{\cosh 2\alpha - \cos 2\beta}. \quad \text{(A.133)}$$

Performing some algebra, we have

$$\begin{aligned}\int_0^{t_r}|Y_x|^2 dy =& \frac{B_{gm}^2}{2\alpha\beta t_r}\left(\frac{\tau}{\pi}\right)^2\eta\frac{-\beta\sinh 2\alpha+\alpha\sin 2\beta}{\cosh 2\alpha-\cos 2\beta} + \frac{B_{gm}^2}{t_r}\left(\frac{\tau}{\pi}\right)^2\frac{\alpha\sinh 2\alpha+\beta\sin 2\beta}{\cosh 2\alpha-\cos 2\beta}\\ =& \frac{B_{gm}^2 t_r}{2\alpha\beta}\left[1+\left(\frac{\tau}{\pi}\right)^2\sigma s\omega_b\mu\sin\delta\right]\cdot \frac{-\beta\sinh 2\alpha+\alpha\sin 2\beta}{\cosh 2\alpha-\cos 2\beta} + \frac{B_{gm}^2}{t_r}\left(\frac{\tau}{\pi}\right)^2\frac{\alpha\sinh 2\alpha+\beta\sin 2\beta}{\cosh 2\alpha-\cos 2\beta}.\end{aligned} \quad \text{(A.134)}$$

And,

$$\int_0^{t_r}|Y_y|^2 dy = \frac{B_{gm}^2}{2}\frac{(t_r/2\alpha)\sinh 2\alpha-(t_r/2\beta)\sin 2\beta}{\cosh 2\alpha-\cos 2\beta} = \frac{B_{gm}^2 t_r}{2\alpha\beta}\frac{\beta\sinh 2\alpha-\alpha\sin 2\beta}{\cosh 2\alpha-\cos 2\beta}. \quad \text{(A.135)}$$

The sum of the integrals is

$$\int_0^{t_r}\left(|Y_x|^2+|Y_y|^2\right)dy = \frac{B_{gm}^2 t_r}{2\alpha\beta}\left(\frac{\tau}{\pi}\right)^2\sigma s\omega_b\mu\sin\delta\frac{-\beta\sinh 2\alpha+\alpha\sin 2\beta}{\cosh 2\alpha-\cos 2\beta} + \frac{B_{gm}^2}{t_r}\left(\frac{\tau}{\pi}\right)^2\frac{\alpha\sinh 2\alpha+\beta\sin 2\beta}{\cosh 2\alpha-\cos 2\beta}. \quad \text{(A.136)}$$

From (A.81), we have

$$\begin{aligned}\int_0^{t_r}\left(|Y_x|^2+|Y_y|^2\right)dy =& \frac{B_{gm}^2 t_r}{t_r}\left(\frac{\tau}{\pi}\right)^2(\tan\delta)\frac{-\beta\sinh 2\alpha+\alpha\sin 2\beta}{\cosh 2\alpha-\cos 2\beta} + \frac{B_{gm}^2}{t_r}\left(\frac{\tau}{\pi}\right)^2\frac{\alpha\sinh 2\alpha+\beta\sin 2\beta}{\cosh 2\alpha-\cos 2\beta}\\ =& \frac{B_{gm}^2}{t_r}\left(\frac{\tau}{\pi}\right)^2\left[\frac{(-\beta\sinh 2\alpha+\alpha\sin 2\beta)\tan\delta}{\cosh 2\alpha-\cos 2\beta} + \frac{\alpha\sinh 2\alpha+\beta\sin 2\beta}{\cosh 2\alpha-\cos 2\beta}\right].\end{aligned} \quad \text{(A.137)}$$

Finally, from (A.125), we have

$$F_H = \frac{p\ell B_{gm}^2\tau^2\sin\delta}{\pi\mu t_r}\left[\frac{(-\beta\sinh 2\alpha+\alpha\sin 2\beta)\tan\delta}{\cosh 2\alpha-\cos 2\beta} + \frac{\alpha\sinh 2\alpha+\beta\sin 2\beta}{\cosh 2\alpha-\cos 2\beta}\right]. \quad \text{(A.138)}$$

A.2.4 Eddy Current Derivation

From (A.42) we have that the induced eddy current density $\mathbf{I}$ is given by

$$\mathbf{I} = \nabla\times\mathbf{H}. \quad \text{(A.139)}$$

From (A.39) we have

$$\mathbf{I} = \frac{1}{\mathring{\mu}}\nabla\times\mathbf{B}. \quad \text{(A.140)}$$

Because we neglected edge effects, we have that $B_z = 0$. Therefore,

$$I_x = 0, \quad I_y = 0. \quad \text{(A.141)}$$

And, the only non-zero component is in the z direction:

$$I_z = \frac{1}{\mathring{\mu}} \left(\frac{\partial B_y}{\partial x} - \frac{\partial B_x}{\partial y} \right). \tag{A.142}$$

Substituting the field solution (A.59), we have

$$I_z = \frac{1}{\mathring{\mu}} \left((-j\pi/\tau) Y_y - \frac{\partial Y_x}{\partial y} \right) e^{j(s\omega_b t - \pi x/\tau - \varphi_o)}. \tag{A.143}$$

Substituting (A.64) and (A.68), we have that

$$\begin{aligned} I_z =& \frac{B_{gm}}{\mathring{\mu}\sqrt{2}\sinh(c)} \Bigg[(-j\pi/\tau) j \sinh(cy/t_r) \\ & - \frac{\tau c^2}{\pi t_r^2} \sinh(cy/t_r) \Bigg] e^{j(s\omega_b t - \pi x/\tau - \varphi_o)} \\ =& \frac{B_{gm} \sinh(cy/t_r)}{\mathring{\mu}\sqrt{2}\sinh(c)} \left(\frac{\pi}{\tau} - \frac{\tau c^2}{\pi t_r^2} \right) e^{j(s\omega_b t - \pi x/\tau - \varphi_o)}. \end{aligned} \tag{A.144}$$

From (A.62) we have

$$I_z = -j \frac{B_{gm} \sinh(cy/t_r)}{\sqrt{2}\sinh(c)} \frac{\tau}{\pi} \sigma s \omega_b e^{j(s\omega_b t - \pi x/\tau - \varphi_o)}. \tag{A.145}$$

Or, simply,

$$I_z = -\frac{\tau \sigma s \omega_b}{\pi} B_y. \tag{A.146}$$

A.2.5 Eddy Force Derivation

The vector force on a conductor with current I in a magnetic field $\mathbf{B}$ is given by the cross-product:

$$\mathbf{F} = \mathrm{Re}(\mathbf{I}) \times \mathrm{Re}(\mathbf{B}). \tag{A.147}$$

Therefore, the eddy force dF_E in the x-direction on an infinitesimal rotor volume element $dxdydz$ is given by

$$dF_E = -\mathrm{Re}(I_z)\mathrm{Re}(B_y) dxdydz. \tag{A.148}$$

Substituting (A.146) gives

$$dF_E = \frac{\tau \sigma s \omega_b}{\pi} (\mathrm{Re} B_y)^2 dxdydz. \tag{A.149}$$

From identity (A.120) we have

$$dF_E = \frac{\tau \sigma s \omega_b}{2\pi} \left[\mathrm{Re}(B_y^2) + |B_y|^2 \right] dxdydz. \tag{A.150}$$

Upon integration w.r.t. x, the first term in the RHS vanishes and the second term is independent of x. Thus, the total eddy current force is

$$\begin{aligned} F_E =& p \int_0^\ell \int_0^{t_r} \int_0^{2\tau} dF_E dxdydz \\ =& \frac{p\ell\tau^2 \sigma s \omega_b}{\pi} \int_0^{t_r} |B_y|^2 dy \\ =& \frac{p\ell\tau^2 \sigma s \omega_b}{\pi} \int_0^{t_r} |Y_y|^2 dy. \end{aligned} \tag{A.151}$$

From (A.135) and (A.81), we have

$$F_E = \frac{\ell\tau^2 \sigma s \omega_b}{\pi} \frac{B_{gm}^2 t_r}{2\alpha\beta} \frac{\beta \sinh 2\alpha - \alpha \sin 2\beta}{\cosh 2\alpha - \cos 2\beta}. \tag{A.152}$$

From (A.81), we have

$$\begin{aligned} F_E =& \frac{p\ell\tau^2 \sigma s \omega_b}{\pi} \frac{B_{gm}^2 t_r}{t_r^2 \sigma s \omega_b \mu \cos\delta} \frac{\beta \sinh 2\alpha - \alpha \sin 2\beta}{\cosh 2\alpha - \cos 2\beta} \\ =& \frac{p\ell\tau^2 B_{gm}^2}{\pi t_r \mu \cos\delta} \frac{\beta \sinh 2\alpha - \alpha \sin 2\beta}{\cosh 2\alpha - \cos 2\beta}. \end{aligned} \tag{A.153}$$

Note: the above vanishes under no slip ($s = 0$), as it should, because it can be seen that $\beta = 0$ when $s = 0$.

A.2.6 Derivation of Parallel Circuit

Hysteresis Components

The total power produced by hysteresis is

$$P_H + W_H = m E_1^2 / R_H \ , \tag{A.154}$$

where E_1 is the electromotive force.

Eq. (26) of MK66,

$$W_H = P_H s/(1-s) \ , \tag{A.155}$$

implies that

$$P_H + W_H = P_H/(1-s). \tag{A.156}$$

Eq. (23) of MK66 is

$$P_H = \frac{B_{gm}^2 \omega_b (1-s) p \tau^3 \ell \sin\delta}{\pi^2 t_r \mu} f(s), \qquad \text{(A.157)}$$

with

$$f(s) \equiv \frac{[\alpha \sin 2\beta - \beta \sinh 2\alpha] \tan\delta}{\cosh 2\alpha - \cos 2\beta} + \frac{\alpha \sin 2\alpha + \beta \sinh 2\beta}{\cosh 2\alpha - \cos 2\beta}. \qquad \text{(A.158)}$$

Thus,

$$P_H + W_H = \frac{B_{gm}^2 \omega_b p \tau^3 \ell \sin\delta}{\pi^2 t_r \mu} f(s). \qquad \text{(A.159)}$$

Solving for R_H in (A.154), we have

$$R_H = \frac{m E_1^2 \pi^2 t_r \mu}{B_{gm}^2 \omega_b p \tau^3 f(s) \ell \sin\delta}. \qquad \text{(A.160)}$$

Eq. (20) of MK66 is

$$B_{gm} = \frac{\pi E_1}{\sqrt{2} \omega_b K_w N_w \tau \ell}\ . \qquad \text{(A.161)}$$

Thus,

$$R_H = \frac{m \omega_b K_w^2 N_w^2 \mu V_r}{p^2 \tau^2 f(s) \sin\delta}, \qquad \text{(A.162)}$$

where the annular ring volume is

$$V_r = 2 p \tau t_r \ell. \qquad \text{(A.163)}$$

Eddy Current Components

Total power from eddy current:

$$P_E + W_E = m E_1^2 / (R_E / s). \qquad \text{(A.164)}$$

Eq. (32) of MK66 is

$$W_E = P_E s / (1-s), \qquad \text{(A.165)}$$

so that

$$P_E + W_E = P_E / (1-s). \qquad \text{(A.166)}$$

Eq. (29) of MK66 is

$$P_E = \frac{B_{gm}^2 \omega_b s (1-s) p \tau^3 \ell t_r \sigma}{2\pi^2} g(s), \qquad \text{(A.167)}$$

where

$$g(s) \equiv \frac{\beta \sinh 2\alpha - \alpha \sin 2\beta}{\alpha\beta(\cosh 2\alpha - \cos 2\beta)}. \qquad \text{(A.168)}$$

Solving for R_E from (A.164),

$$R_E = \frac{2\pi^2 m E_1^2}{B_{gm}^2 \omega_b^2 \tau^3 p t_r \ell \sigma g(s)}. \qquad \text{(A.169)}$$

Substituting for B_{gm} from (A.161), we have

$$R_E = \frac{4 m K_w^2 N_w^2 \ell}{p \tau t_r \sigma g(s)}. \qquad \text{(A.170)}$$

Appendix B

Appendix: Expressions for Torque

B.1 In the Stationary Frame

In keeping with the notation in Miyairi and Kataoka (1965), we define the "gap currents", which are the currents passing through the inductor L_m, by[1]

$$i_{dg} \equiv i_{ds} + i_{dr}, \tag{B.1}$$
$$i_{qg} \equiv i_{qs} + i_{qr}. \tag{B.2}$$

For balanced input, in the stationary frame, we have

$$i_{ds} = I_s \cos(\omega_b t),$$
$$i_{qs} = -I_s \sin(\omega_b t).$$

By examining the relevant phase shifts in (A.26) and (A.27) with respect to the input, we have

$$i_{dg} = I_g \cos(\omega_b t + \varphi_o), \tag{B.3}$$
$$i_{dr} = I_r \cos(\omega_b t + \delta + \varphi_o), \tag{B.4}$$
$$i_{qg} = -I_g \sin(\omega_b t + \varphi_o), \tag{B.5}$$
$$i_{qr} = -I_r \sin(\omega_b t + \delta + \varphi_o). \tag{B.6}$$
$$\tag{B.7}$$

B.1.1 Torque in Terms of Currents

Miyairi and Kataoka (1965) show that the torque output of the motor is

$$T_e = \frac{pV_r B_m^2}{2\mu} \sin\delta = \frac{pV_r S_H}{2\pi}, \tag{B.8}$$

where $p = P/2$ is the number of pole pairs, and

$$S_H = \frac{\pi B_m^2}{\mu} \sin\delta \tag{B.9}$$

is the area of the hysteresis ellipse, and the volume of the ring is

$$V_r = 2\pi r_r t_r \ell. \tag{B.10}$$

From (A.26) and (A.27) we have

$$I_g = \frac{B_m \ell_g p^2 t_r \pi}{m\mu_o r_g K_w N_w}, \tag{B.11}$$

$$I_r = \frac{B_m r_r \pi}{m\mu K_w N_w}. \tag{B.12}$$

And, from (A.31), we have

$$L_m = L_g = \frac{2\ell r_g K_w^2 N_w^2 m\mu_o}{p^2 \pi \ell_g}. \tag{B.13}$$

Therefore,

$$L_m I_g I_r = \frac{2\pi \ell t_r r_r B_m^2}{m\mu} = \frac{V_r B_m^2}{m\mu}. \tag{B.14}$$

From (B.8), we have

$$T_e = \frac{m}{2} p L_m I_g I_r \sin\delta. \tag{B.15}$$

The currents I_g and I_r are found from Eqs. (B.3)-(B.6), which give

$$I_r = \sqrt{i_{dr}^2 + i_{qr}^2}, \tag{B.16}$$

$$I_g = \sqrt{i_{dg}^2 + i_{qg}^2}. \tag{B.17}$$

B.1.2 Torque in Terms of Flux and Currents

From (4.41) and (4.45), the flux linkages are

$$\lambda_{dr} = (L_{hr} + L_m)i_{dr} + L_m i_{ds}, \tag{B.18}$$
$$\lambda_{qr} = (L_{hr} + L_m)i_{qr} + L_m i_{qs}. \tag{B.19}$$

The torque "cross term" expression can be seen to equal

$$\begin{aligned}(\lambda_{qr}i_{dr} - \lambda_{dr}i_{qr}) &= L_m(i_{qs}i_{dr} - i_{ds}i_{qr}) \\ &= L_m(i_{qg} - i_{qr})i_{dr} - L_m(i_{dg} - i_{dr})i_{qr} \\ &= L_m(i_{qg}i_{dr} - i_{dg}i_{qr}).\end{aligned} \tag{B.20}$$

We, then, have

$$\begin{aligned}&pL_m(i_{qg}i_{dr} - i_{dg}i_{qr}) = \\ &\quad pL_m I_g I_r \Big[-\sin(\omega_b t + \varphi_o)\cos(\omega_b t + \delta + \varphi_o) \\ &\qquad + \cos(\omega_b t + \varphi_o)\sin(\omega_b t + \delta + \varphi_o)\Big] \\ &= pL_m I_g I_r \sin((\omega_b t + \delta + \varphi_o) - (\omega_b t + \varphi_o)) \\ &= pL_m I_g I_r \sin\delta.\end{aligned} \tag{B.21}$$

From (B.15), we have the expression for the torque

$$T_e = \frac{m}{2} pL_m(i_{qg}i_{dr} - i_{dg}i_{qr}). \tag{B.22}$$

Hence, from (B.20), we have

$$T_e = \frac{m}{2} p(\lambda_{qr}i_{dr} - \lambda_{dr}i_{qr}). \tag{B.23}$$

B.2 In the Rotating Frame

In the frame rotating with the stator field, for a balanced 3-phase input, the input current is

$$i_{ds} = I_o\cos(\varphi_o), \quad i_{qs} = -I_o\sin(\varphi_o). \tag{B.24}$$

By examining the relevant phase shifts in (A.26) and (A.27) with respect to the input, we have

$$\begin{aligned}i_{dg} &= I_g\cos(\varphi_o), \\ i_{dr} &= I_r\cos(\delta + \varphi_o), \\ i_{qg} &= -I_g\sin(\varphi_o), \\ i_{qr} &= -I_r\sin(\delta + \varphi_o).\end{aligned} \tag{B.25}$$

By duplicating steps in the derivations for the stationary frame, we obtain the same form of the expressions:

$$T_e = \frac{m}{2} pL_m I_g I_r \sin\delta, \tag{B.26}$$

and

$$T_e = \frac{m}{2} p(\lambda_{qr}i_{dr} - \lambda_{dr}i_{qr}). \tag{B.27}$$

Appendix C

Appendix: Derivation of Magnetomotive Force Expression

Assume complex currents in the stator of the form:

$$\mathring{I}^{(k)} = Ie^{j(\omega t - \psi_k)}. \tag{C.1}$$

where I is real. The resulting complex magnetomotive force is

$$\begin{aligned}
\mathring{F} &= \sum_{k=1}^{m} \mathring{I}^{(k)} W \cos(\psi - \psi_k) \\
&= IW \sum_{k=1}^{m} \mathring{I}^{(k)} e^{j(\omega t - \psi_k)} \cos(\psi - \psi_k) \\
&= \frac{1}{2} IW \sum_{k=1}^{m} e^{j(\omega t - \psi_k)} \left(e^{j(\psi - \psi_k)} + e^{-j(\psi - \psi_k)} \right) \\
&= \frac{1}{2} IW \sum_{k=1}^{m} \left(e^{j(\omega t + \psi - 2\psi_k)} + e^{j(\omega t - \psi)} \right) \\
&= \frac{1}{2} IW \cdot \left(e^{j(\omega t + \psi)} \sum_{k=1}^{m} e^{-2j\psi_k} + m e^{j(\omega t - \psi)} \right).
\end{aligned} \tag{C.2}$$

The sum that is in the RHS can be written as

$$\sum_{k=1}^{m} e^{-2j\psi_k} = \sum_{k=1}^{m} a^{k-1} = \frac{a^m - 1}{a - 1}, \tag{C.3}$$

where

$$a \equiv e^{-4\pi j/m}. \tag{C.4}$$

Since

$$a^m = e^{-4\pi j} = \cos 4\pi + j \sin 4\pi = 1, \tag{C.5}$$

we have that the sum vanishes:

$$\sum_{k=1}^{m} e^{-2j\psi_k} = 0. \tag{C.6}$$

Thus,

$$\mathring{F} = \frac{m}{2} IW e^{j(\omega t - \psi)}. \tag{C.7}$$

The real part of the magnetomotive force is, therefore,

$$F = \frac{m}{2} IW \cos(\omega t - \psi). \tag{C.8}$$